

# Search for heavy Majorana neutrinos in the $\tau$ final state at proton-electron colliders

Haiyong Gu<sup>a,b</sup>, Ying-nan Mao<sup>a</sup>, Hao Sun<sup>c</sup> and Kechen Wang<sup>a,1</sup>

<sup>a</sup>*Department of Physics, School of Science, Wuhan University of Technology,  
430070 Wuhan, Hubei, China*

<sup>b</sup>*School of Information Science and Technology, Xiamen University Tan Kah Kee College,  
363105 Zhangzhou, Fujian, China*

<sup>c</sup>*Institute of Theoretical Physics, School of Physics, Dalian University of Technology,  
116024 Dalian, Liaoning, China*

*E-mail:* [haiyong@xujc.com](mailto:haiyong@xujc.com), [ynmao@whut.edu.cn](mailto:ynmao@whut.edu.cn), [haosun@dlut.edu.cn](mailto:haosun@dlut.edu.cn),  
[kechen.wang@whut.edu.cn](mailto:kechen.wang@whut.edu.cn)

**ABSTRACT:** We utilize the lepton number violation signal process  $pe^- \rightarrow \tau^+ jjj$  to search for heavy Majorana neutrinos at future proton-electron colliders. The LHeC (FCC-eh) is considered to run with an electron beam energy of 60 GeV, a proton beam energy of 7 (50) TeV and an integrated luminosity of 1 (3)  $\text{ab}^{-1}$ , and the electron beam is considered to be unpolarized. We apply detector configurations and simulate signal and related standard model background events for both hadronic  $\tau_h$  and leptonic  $\tau_\ell$  final states,  $\ell$  being a muon. After preselection, multivariate analyses are performed to reject the background. The strategy to reconstruct the heavy neutrino mass is developed and distributions of reconstructed mass are presented. Discovery sensitivities on parameter  $|V_{\tau N}|^2 |V_{eN}|^2 / (|V_{\tau N}|^2 + |V_{eN}|^2)$  for the heavy neutrino mass between 10 and 3000 GeV are predicted. At the  $2\text{-}\sigma$  significance, the best discovery sensitivity is  $\sim 1.2 \times 10^{-5}$  ( $5.0 \times 10^{-6}$ ) at the LHeC (FCC-eh) when  $m_N \sim 100$  GeV for the hadronic  $\tau_h$  final state. Sensitivities for the leptonic  $\tau_\ell$  final state are found to be similar to those for the hadronic  $\tau_h$  final state for most of the parameter space investigated. We also derive the limits on mixing parameters from electroweak precision data (EWPD) and DELPHI experiment. Assuming  $|V_{\tau N}|^2 = |V_{eN}|^2 = |V_{\ell N}|^2$ , sensitivity bounds from the LHeC and FCC-eh experiments are found to be stronger than those from EWPD when  $m_N \lesssim 900$  GeV, and also stronger than those from DELPHI when  $m_N \gtrsim 70$  GeV. Constraints are also interpreted and compared in the  $|V_{\tau N}|^2$  vs.  $|V_{eN}|^2$  plane. Compared with current limits from EWPD, DELPHI, and LHC experiments, future  $pe$  experiments can probe large additional regions in the parameter space formed by  $|V_{\tau N}|^2$  and  $|V_{eN}|^2$ , and thus significantly enhance the discovery potential for a large portion of the  $|V_{\tau N}|^2$  vs.  $|V_{eN}|^2$  plane.

<sup>1</sup>Corresponding author.

---

## Contents

<b>1</b>	<b>Introduction</b>	<b>1</b>
<b>2</b>	<b>The signal production process</b>	<b>3</b>
<b>3</b>	<b>Hadronic <math>\tau_h</math> final state</b>	<b>5</b>
3.1	SM background processes	5
3.2	Data analysis	6
<b>4</b>	<b>Leptonic <math>\tau_\mu</math> final state</b>	<b>8</b>
4.1	SM background processes	8
4.2	Data analysis	8
<b>5</b>	<b>Results</b>	<b>10</b>
<b>6</b>	<b>Sensitivities compared with current experimental limits</b>	<b>13</b>
<b>7</b>	<b>Conclusion and discussion</b>	<b>15</b>
<b>A</b>	<b>Constraints from <math>Z \rightarrow N\nu, N\bar{\nu}</math> rare decay channels and EWPD</b>	<b>16</b>
<b>B</b>	<b>Distributions of BDT responses</b>	<b>20</b>
B.1	Hadronic $\tau_h$ final state	20
B.2	Leptonic $\tau_\mu$ final state	21
<b>C</b>	<b>Distributions of representative high-level observables</b>	<b>24</b>
C.1	Hadronic $\tau_h$ final state	24
C.2	Leptonic $\tau_\mu$ final state	27
<b>D</b>	<b>The Selection efficiency tables</b>	<b>30</b>
D.1	Hadronic $\tau_h$ final state	30
D.2	Leptonic $\tau_\mu$ final state	30

---

## 1 Introduction

The experiments of neutrino oscillation [1–6] show that at least two of three active neutrinos are massive. However, in the standard model (SM), neutrinos have only left-handed components and no right-handed components, so they cannot form a Dirac mass term, and the neutrino mass is strictly equal to zero. Therefore, the standard model needs to be

slightly expanded. One important method is the seesaw mechanism [7–17], which introduces right-handed Majorana neutrinos  $N_R$  and couple them with SM neutrinos to produce small neutrino masses  $M_{\nu} \sim M_D^2/M_R$ , where  $M_R$  is the Majorana mass of  $N_R$  and  $M_D$  is the Dirac mass and proportional to the Yukawa coupling between the standard model neutrino and  $N_R$ . When  $M_R \gg M_D$ , active neutrino acquires a small mass.

Search for the heavy neutrinos is crucial to verify the seesaw mechanism. Because the production cross section, decay width, and lifetime of  $N$  are determined by its mass  $m_N$  and the parameter  $|V_{\ell N}|^2$  which is related to the matrix element describing the mixing of  $N$  with the SM neutrino of flavor  $\ell = e, \mu, \tau$ , limits for such searches are usually given in the plane of the mixing parameter  $|V_{\ell N}|^2$  vs.  $m_N$ .

At colliders, they can be searched from the decays of Higgs bosons [18, 19],  $W$ -bosons [20–23] and  $Z$ -bosons [24]. Summaries of collider searches of heavy neutrinos can be found in Refs. [25–33] and references therein. Recent experimental studies on heavy neutrino searches can be found in Refs. [34–44], and are reviewed in Ref. [45].

Compared with plentiful studies focusing on the mixing parameters  $|V_{eN}|^2$  and  $|V_{\mu N}|^2$ , because of the challenges in detecting the final state taus, the mixing parameter  $|V_{\tau N}|^2$  is more difficult to be probed, making it not well studied at current experiments. For heavy neutrinos with mass above 10 GeV, the main experimental constraints on the mixing parameter  $|V_{\tau N}|^2$  are set by the DELPHI [46], and can be derived from the electroweak precision data (EWPD) [47–53] and rare decays of  $Z$ -boson [46].

However, in phenomenology, there do exist some studies to probe the mixing parameter  $|V_{\tau N}|^2$  in different heavy neutrino mass ranges. Among them, Refs. [54–57] study heavy neutrinos with  $m_N \sim (0.1 - 5)$  GeV; Refs. [58, 59] for  $m_N \sim (1 - 20)$  GeV; Ref. [53] for  $m_N \sim (25 - 150)$  GeV; and Refs. [60–62] for  $m_N > 150$  GeV. In the recent work [63], some of our authors derive current constraints on  $|V_{\tau N}|^2$  from the rare  $Z$ -boson decay and electroweak precision data (EWPD), and forecast sensitivities on  $|V_{\tau N}|^2$  via the signal  $pp \rightarrow \tau^\pm \tau^\pm jj$  at future proton-proton colliders.

Ref. [64] and references therein have reviewed BSM physics searches at future electron-proton colliders, the Large Hadron electron Collider (LHeC) [65–70] and the electron-hadron mode of the Future Circular Collider (FCC-eh) [68, 70–73]. The  $\tau$  final state at  $pe$  colliders is also studied in Ref. [74]. Phenomenology studies on heavy neutrino searches at  $ep$  colliders can be found in Refs. [45, 75–90].

Among them, in Ref. [45], some of our authors develop the search strategy for a heavy Majorana neutrino via the lepton number violation signal process  $pe^- \rightarrow \mu^+ jjj$  at future electron-proton colliders. Assuming mixing parameters  $|V_{\ell N}|^2 = |V_{\mu N}|^2 = |V_{eN}|^2$  and  $|V_{\tau N}|^2 = 0$ , the dominant SM background processes are considered, and discovery sensitivities on the mixing parameter  $|V_{\ell N}|^2$  are predicted for the heavy neutrino mass in the range of 10-3000 GeV. The results show that the sensitivities at electron-proton colliders are much stronger than the current experimental limits at the LHC for  $m_N$  above 30 GeV.

In this consecutive study, we concentrate on the signal process  $pe^- \rightarrow \tau^+ jjj$  with final state taus at the LHeC and FCC-eh. Similar to Ref. [45], the LHeC (FCC-eh) is supposed

to run with an electron beam energy of 60 GeV, a proton beam energy of 7 (50) TeV and an integrated luminosity of 1 (3)  $\text{ab}^{-1}$ ; the electron beam is considered to be unpolarized; and to simplify the analyses, we consider the phenomenological simplified Type-I model and the scenario that only one generation of heavy neutrinos  $N$  is within the collider access. The  $N$  is assumed to mix with active neutrinos of tau and electron flavours, i.e.  $|V_{\tau N}|^2, |V_{eN}|^2 \neq 0$  and  $|V_{\mu N}|^2 = 0$ .

Since taus are unstable, they decay either leptonically into muons and electrons, or hadronically into mesons, leading to final state leptons or tau-jets at colliders. Because leptonic and hadronic final states have different kinematics and background, to obtain and compare the sensitivities for both states, we perform their analyses individually and forecast sensitivities for heavy neutrinos in the range 10-3000 GeV at LHeC and FCC-eh.

The organization of our paper is as follows. In Sec. 2, we present the cross section of the signal process. In Sec. 3 and Sec. 4, we show the SM background processes and the analyses for the hadronic and leptonic final states, respectively. In Sec. 5, we present sensitivity curves in the mixing parameters vs. heavy neutrino mass plane at the LHeC and FCC-eh. The sensitivities obtained from this study are compared with those from current experiments in Sec. 6. We conclude in Sec. 7. Details of this study are listed in Appendices A–D.

## 2 The signal production process

As shown in Fig. 1, heavy Majorana neutrinos  $N$  can be produced via the  $t$ -channel exchange of  $W$  bosons at the  $pe$  colliders, and decay finally into  $\tau^+$  plus three jets. The lepton number of this process changes from  $+1$  to  $-1$ , so it violates the conservation of lepton number.

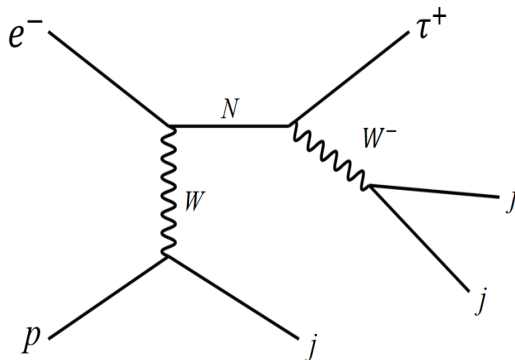


**Figure 1:** The production process of the Lepton Number Violating (LNV) signal in the tau final state via the heavy Majorana neutrinos at  $pe$  colliders.

For the data simulation, we implement the Universal FeynRules Output model file [91, 92] which extends the SM with additional heavy neutrinos interacting with active neutrinos into MadGraph5 [93] to generate the signal events. When generating collision events, the

default “nn23lo1” parton distribution function of the proton is used. To maximize the event acceptance, following loose requirements are applied at the parton level in MadGraph (implemented in the run\_card.dat file) for both the signal and background: the minimal value of transverse momentum for the jet (lepton) is set to be 5 (2) GeV; the pseudorapidity ( $\eta$ ) range for both the lepton and jet is set to be  $|\eta| < 10$ ; the minimal value of the solid angular distance,  $\Delta R = \sqrt{\Delta\eta^2 + \Delta\phi^2}$ , between final state objects is set to be 0.01.

Similar to our previous work [19, 94], the Pythia6 [95] program is modified to perform the parton showering and the hadronization for the  $pe$  colliders, while the configuration card files [96] for the LHeC and FCC-eh detectors are implemented to the Delphes program [97] to complete the detector simulation. For the jet reconstruction, jets are classified by using the FastJet package [98] with anti- $k_t$  algorithm and cone radius  $R = 0.4$ . For the final state tau reconstruction, the default rates in the Delphes configuration card files are used, where the identification efficiency for tau-tagging is set to be 40%, and the misidentification rate is set to be about 0.1%.

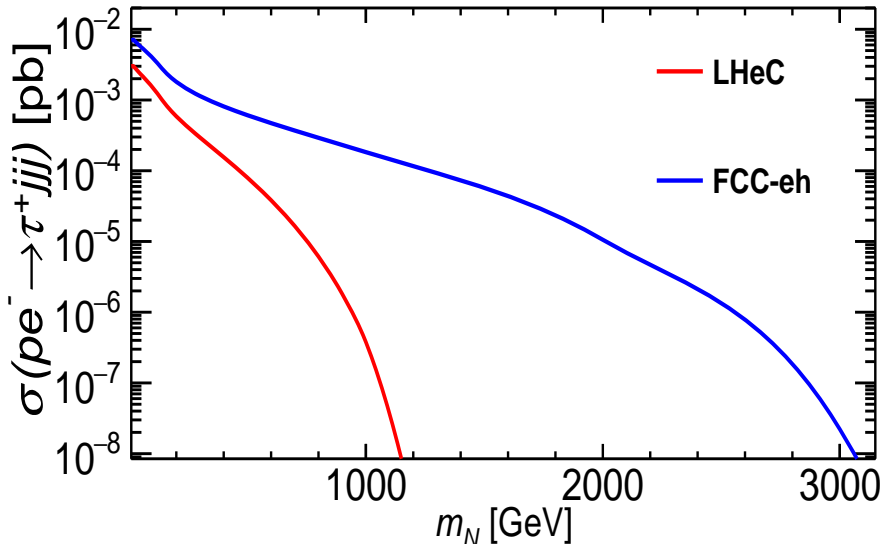


**Figure 2:** The production cross section of the LNV signal  $pe^- \rightarrow \tau^+ jjj$  via the heavy Majorana neutrino  $N$  when fixing  $|V_{\tau N}|^2 |V_{eN}|^2 / (|V_{\tau N}|^2 + |V_{eN}|^2) = 5 \times 10^{-5}$  and varying  $m_N$  at the LHeC and FCC-eh.

For the signal data simulation, we fix the benchmark mixing parameter  $|V_{\ell N}|^2 = |V_{eN}|^2 = |V_{\tau N}|^2 = 10^{-4}$ , and vary the heavy neutrino mass  $m_N$ . At the LHeC (FCC-eh), when  $m_N = 10$  and 20 GeV, we generate 15.3 (7.8) and 3.3 (1.8) million signal events, respectively, while 0.3 (0.6) million signal events are generated when  $m_N = 40, 60, 70, 100, 120, 200, 300, 400, 500, 600, 700, 800, 900, 1000$  GeV. Besides, at the LHeC, 0.3 million signal events are generated for one additional mass point with  $m_N = 1150$  GeV, while at the FCC-eh, 0.6 million signal events are generated for two additional mass points with  $m_N$

= 2000 and 3150 GeV.

To maintain consistency through this study, the production cross sections calculated by MadGraph5 are used to estimate the number of events for both the signal and the background processes. In Fig. 2, we plot the cross sections of the LNV signal  $pe^- \rightarrow \tau^+ jjj$  via the Majorana heavy neutrino  $N$  as a function of heavy neutrino mass  $m_N$  at the LHeC and FCC-eh. The signal productions are proportional to the parameter  $|V_{\tau N}|^2 |V_{eN}|^2 / (|V_{\tau N}|^2 + |V_{eN}|^2)$  which is fixed to be  $5 \times 10^{-5}$  in Fig. 2. For large  $m_N$  the cross sections for LHeC decrease much faster than those for FCC-eh. This behaviour can be understood from the parton distribution function of the proton, and is explained in details in Ref. [45].

### 3 Hadronic $\tau_h$ final state

#### 3.1 SM background processes

When tau decays hadronically, the final state contains one tau-jet  $\tau_h$  with positive charge, at least three regular jets and missing energy. There exist four types of background processes:  $pe^- \rightarrow \tau^+ \tau^- e^- jjj$ ,  $\tau^+ \tau^- \nu_e jjj$ ,  $\tau^+ \nu_\tau e^- jjj$ , and  $\tau^+ \nu_\tau \nu_e jjj$ , which we label as “B1-B4” in this article. They can have the similar final state as the signal when the final state  $\tau^-$  and  $e^-$  are undetected. Besides, because the jet production is still substantial at  $pe$  colliders, the misidentified taus from jets needs to be considered. The multi-jet process “ $pe^- \rightarrow \nu_e jjjj$  with a  $j \rightarrow \tau_h^+$ ” is the main background of such kind, and is labeled as “B5a”. The Delphes configuration card files [96] are used for the LHeC and FCC-eh detector simulations in this study, and the misidentification rate for the tau-tagging is set to be about 0.1% in these files. Therefore, we use this value as benchmark to test the effect of misidentified tau-jets.

Table 1 shows the production cross sections of background processes at the LHeC and FCC-eh for the hadronic  $\tau_h$  final state. Among them,  $\nu_e jjjj$  has the largest cross sections without any requirements, followed by  $\tau^+ \tau^- e^- jjj$  and  $\tau^+ \nu_\tau e^- jjj$ . For the remaining two background processes, due to their small cross sections, they do not play a dominant role.

	$\sigma$ [pb]	LHeC	FCC-eh
B1	$\tau^+ \tau^- e^- jjj$	0.22	0.86
B2	$\tau^+ \tau^- \nu_e jjj$	0.052	0.29
B3	$\tau^+ \nu_\tau e^- jjj$	0.28	1.6
B4	$\tau^+ \nu_\tau \nu_e jjj$	$8.2 \times 10^{-6}$	$9.3 \times 10^{-5}$
B5a	$\nu_e jjjj$	309	1159

**Table 1:** The production cross sections of background processes at the LHeC and FCC-eh for the hadronic  $\tau_h$  final state.

The number of simulated events for each background process is determined according to its importance in reducing the statistical uncertainty of the final sensitivities. At the

LHeC (FCC-eh), we generate 2.1 (1.2) million  $\tau^+\tau^-e^-jjj$ , 4.9 (3.0) million  $\tau^+\tau^-\nu_ejjj$ , 21 (19) million  $\tau^+\nu_\tau e^-jjj$ , 0.5 (0.5) million  $\tau^+\nu_\tau\nu_ejjj$ , and 32 (25) million  $\nu_ejjjj$  events, respectively.

### 3.2 Data analysis

We apply following preselection to select the signal and reject the background events at the first stage. (i) Exactly one  $\tau$ -jet with positive charge, i.e.  $N(\tau_h^+) = 1$  and transverse momentum  $p_T(\tau_h) > 5$  GeV; events with final state electron(s) or muon(s) are vetoed. (ii) All regular jets are sorted in descending order according to their transverse momenta and we require at least three jets, i.e.  $N(j) \geq 3$ ; for the  $p_T$  thresholds of jets, when heavy neutrino mass is below 80 GeV, the  $p_T$  of the first three leading jets are required to be greater than 10 GeV, while when the mass is above 80 GeV, we require the first two leading jets have  $p_T$  greater than 20 GeV and the third one has  $p_T$  greater than 10 GeV. (iii) To reject the background from misidentified taus, the solid angular distance  $\Delta R$  between the regular jet and tau-jet is required to be larger than 0.8, i.e.,  $\Delta R(\tau_h, j) > 0.8$ .

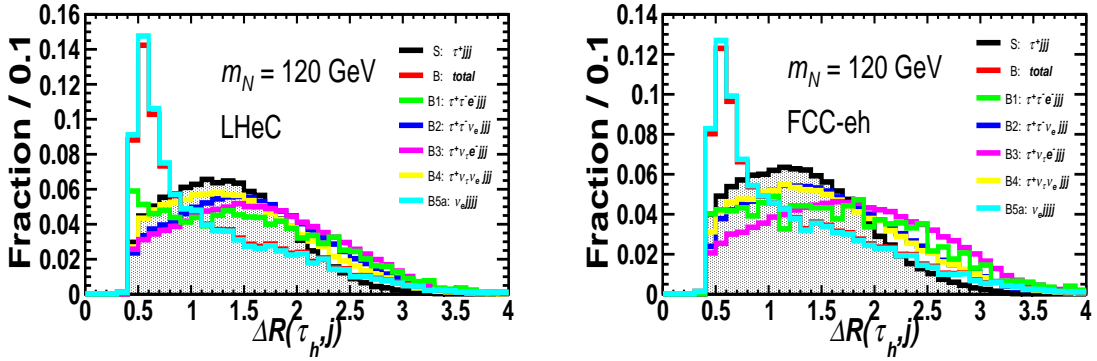


**Figure 3:** The  $\Delta R(\tau_h, j)$  distributions for the signal with benchmark  $m_N = 120$  GeV and  $|V_{\tau N}|^2 |V_{eN}|^2 / (|V_{\tau N}|^2 + |V_{eN}|^2) = 5 \times 10^{-5}$ , and for background processes after applying preselection (i)-(ii) for the hadronic  $\tau_h$  final state at the LHeC and FCC-eh.

To exploit the  $\Delta R(\tau_h, j)$  observable, we calculate  $\Delta R(\tau_h, j)$  values for all possible combinations of tau- and regular jets in the same event, and select the minimal value. Fig. 3 shows the distributions of such minimal  $\Delta R(\tau_h, j)$  for the signal with benchmark  $m_N = 120$  GeV and  $|V_{\tau N}|^2 |V_{eN}|^2 / (|V_{\tau N}|^2 + |V_{eN}|^2) = 5 \times 10^{-5}$ , and for background processes after applying preselection (i)-(ii). One observes that the  $\nu_ejjjj$  process still dominates after applying preselection (i)-(ii), and can be rejected effectively by the  $\Delta R(\tau_h, j)$  requirement.

In Table 2, we show the number of events for the signal with benchmark  $m_N = 120$  GeV and background processes after applying the preselection (i)-(iii) sequentially described above. One observes that, initially at the LHeC (FCC-eh), without any selection, B5a is a factor of 562 (417) larger than the sum of B1-B4, while the ratio is reduced to 21 (23) after

preselection (i)-(ii) and becomes 14 (16) after preselection (iii), which means the preselection rejects B5a effectively.

		signal	B1	B2	B3	B4	B5a
LHeC	initial	$1.2 \times 10^3$	$2.2 \times 10^5$	$5.2 \times 10^4$	$2.8 \times 10^5$	8.2	$3.1 \times 10^8$
	(i)	$2.8 \times 10^2$	$1.6 \times 10^3$	$4.7 \times 10^3$	$5.5 \times 10^3$	1.9	$4.7 \times 10^5$
	(ii)	$2.2 \times 10^2$	$4.3 \times 10^2$	$1.6 \times 10^3$	$1.8 \times 10^3$	1.3	$8.0 \times 10^4$
	(iii)	$1.8 \times 10^2$	$3.4 \times 10^2$	$1.4 \times 10^3$	$1.6 \times 10^3$	1.1	$4.6 \times 10^4$
FCC-eh	initial	$1.0 \times 10^4$	$2.6 \times 10^6$	$8.7 \times 10^5$	$4.9 \times 10^6$	$2.8 \times 10^2$	$3.5 \times 10^9$
	(i)	$2.3 \times 10^3$	$1.4 \times 10^4$	$8.4 \times 10^4$	$8.1 \times 10^4$	63	$6.2 \times 10^6$
	(ii)	$1.9 \times 10^3$	$4.5 \times 10^3$	$3.9 \times 10^4$	$3.5 \times 10^4$	52	$1.8 \times 10^6$
	(iii)	$1.5 \times 10^3$	$3.8 \times 10^3$	$3.3 \times 10^4$	$3.1 \times 10^4$	43	$1.1 \times 10^6$

**Table 2:** The number of events for the signal with benchmark  $m_N = 120$  GeV and  $|V_{\tau N}|^2 |V_{eN}|^2 / (|V_{\tau N}|^2 + |V_{eN}|^2) = 5 \times 10^{-5}$ , and for background processes after applying preselection (i)-(ii) sequentially for the hadronic  $\tau_h$  final state. The numbers correspond to the LHeC and FCC-eh with 1 and 3  $\text{ab}^{-1}$  integrated luminosity, respectively.

To further reject the background, we input following nineteen observables into the Toolkit for Multivariate Analysis (TMVA) package [99] to perform the multivariate analysis (MVA).

- A. Four momenta of the final state  $\tau_h$ :  $p_x(\tau_h), p_y(\tau_h), p_z(\tau_h), E(\tau_h)$ .
- B. Four momenta of the first three final state regular jets:  $p_x(j_1), p_y(j_1), p_z(j_1), E(j_1)$ ;  $p_x(j_2), p_y(j_2), p_z(j_2), E(j_2)$ ;  $p_x(j_3), p_y(j_3), p_z(j_3), E(j_3)$ .
- C. Number of regular jets:  $N(j)$ .
- D. Magnitude and azimuthal angle of the missing transverse momentum:  $\cancel{E}_T, \phi(\cancel{E}_T)$ .
- E. The minimal value of solid angular distances between the final state tau- and regular jets:  $\Delta R(\tau_h, j)$ .

The Boosted Decision Tree (BDT) algorithm is adopted to perform the MVA and maximally reject the background. The default setting in the TMVA package is used, where the number of trees in the forest “NTrees” is set to be 850, the minimum percentage of training events required in a leaf node “MinNodeSize” is set to be 2.5%, the maximal depth of the decision tree allowed “MaxDepth” is set to be 3, the learning rate for AdaBoost algorithm “AdaBoostBeta” is set to be 0.5, the relative size of bagged event sample to original size of the data sample “BaggedSampleFraction” is set to be 0.5, and the number of grid points in variable range used in finding optimal cut in node splitting “nCuts” is set to be 20. In Fig. 4, we show BDT distributions for the total background and the benchmark signal with  $m_N = 120$  GeV at the LHeC and FCC-eh. Since the kinematics of signal



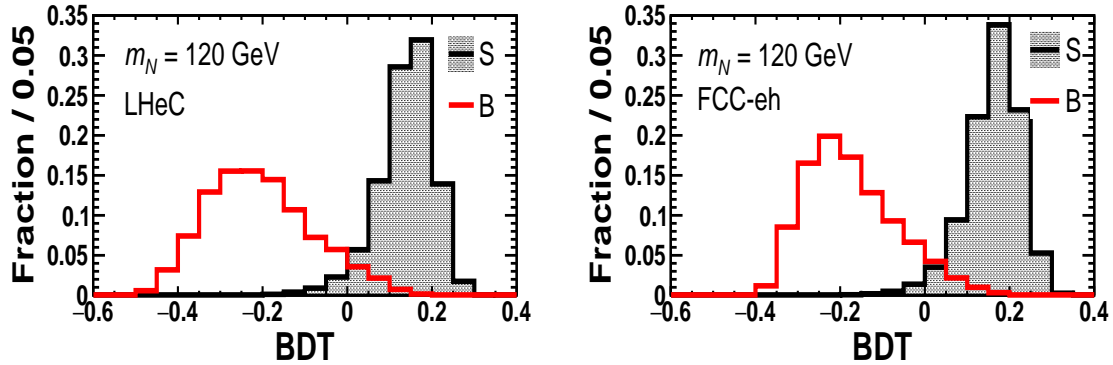


**Figure 4:** Distributions of BDT responses for the signal with benchmark  $m_N = 120$  GeV and  $|V_{\tau N}|^2 |V_{e N}|^2 / (|V_{\tau N}|^2 + |V_{e N}|^2) = 5 \times 10^{-5}$  (black, filled) and for total SM background (red) at the LHeC (left) and FCC-eh (right) for the hadronic  $\tau_h$  final state.

varies with  $m_N$ , distributions of BDT response also change with  $m_N$ . BDT distributions corresponding to other representative heavy neutrino masses are shown in Appendix B.1 for the LHeC and FCC-eh.

## 4 Leptonic $\tau_\mu$ final state

### 4.1 SM background processes

When tau decays leptonically, we select the final state with tau decaying into muons which we label as “ $\tau_\mu$ ” in this article. Thus, signature of final state has one positively charged muon, at least three regular jets plus missing energy. Besides the B1-B4 processes including taus, SM processes including muons can also contribute to the background in this scenario. Therefore, four additional background processes:  $\mu^+ \mu^- e^- jjj$ ,  $\mu^+ \mu^- \nu_e jjj$ ,  $\mu^+ \nu_\mu e^- jjj$ , and  $\mu^+ \nu_\mu \nu_e jjj$  are included, and labelled as “B5-B8” in this article. Table 3 shows the production cross sections of background processes at the LHeC and FCC-eh for the leptonic  $\tau_\mu$  final state.

For the background at the LHeC (FCC-eh), we generate 2.1 (1.2) million  $\tau^+ \tau^- e^- jjj$ , 4.9 (3.0) million  $\tau^+ \tau^- \nu_e jjj$ , 21 (19) million  $\tau^+ \nu_\tau e^- jjj$ , 0.5 (0.5) million  $\tau^+ \nu_\tau \nu_e jjj$ , 2.1 (2.0) million  $\mu^+ \mu^- e^- jjj$ , 10.5 (6.0) million  $\mu^+ \mu^- \nu_e jjj$ , 27.4 (24.6) million  $\mu^+ \nu_\mu e^- jjj$ , 6.0 (6.4) million  $\mu^+ \nu_\mu \nu_e jjj$ , respectively. The number of simulated events for each background process is determined according to its importance in reducing the statistical uncertainty of the final sensitivities.

### 4.2 Data analysis

We apply following preselection to select the signal and reject the background events at the first stage. (i) Exactly one muon with positive charge, i.e.  $N(\tau_\mu^+) = 1$  and transverse momentum  $p_T(\tau_\mu) > 5$  GeV; events with final state electron(s) or tau-jet(s) are vetoed. (ii) All regular jets are sorted in descending order according to their transverse momenta

	$\sigma$ [pb]	LHeC	FCC-eh
B1	$\tau^+\tau^-e^-jjj$	0.22	0.86
B2	$\tau^+\tau^-\nu_ejjj$	0.052	0.29
B3	$\tau^+\nu_\tau e^-jjj$	0.28	1.6
B4	$\tau^+\nu_\tau\nu_ejjj$	$8.2\times 10^{-6}$	$9.3\times 10^{-5}$
B5	$\mu^+\mu^-e^-jjj$	0.58	2.1
B6	$\mu^+\mu^-\nu_ejjj$	$8.6\times 10^{-2}$	0.39
B7	$\mu^+\nu_\mu e^-jjj$	0.28	1.6
B8	$\mu^+\nu_\mu\nu_ejjj$	$8.1\times 10^{-6}$	$9.3\times 10^{-5}$

**Table 3:** The production cross sections of background processes at the LHeC and FCC-eh for the leptonic  $\tau_\mu$  final state.

and we require at least three jets, i.e.  $N(j) \geq 3$ ; for the  $p_T$  thresholds of jets, when heavy neutrino mass is below 80 GeV, the  $p_T$  of the first three leading jets are required to be greater than 10 GeV, while when the mass is above 80 GeV, we require the first two leading jets have  $p_T$  greater than 20 GeV and the third one has  $p_T$  greater than 10 GeV. In Table 4, we show the number of events for the signal with benchmark  $m_N = 120$  GeV and dominant background processes after applying the preselection (i)-(ii) sequentially described above.

		signal	B1	B2	B3	B4	B5	B7
LHeC	initial	$1.2\times 10^3$	$2.2\times 10^5$	$5.2\times 10^4$	$2.8\times 10^5$	8.2	$5.8\times 10^5$	$2.8\times 10^5$
	(i)	$1.2\times 10^2$	$4.1\times 10^2$	$2.1\times 10^3$	$2.6\times 10^3$	$7.6\times 10^{-1}$	$2.6\times 10^3$	$1.9\times 10^4$
	(ii)	$9.9\times 10^1$	$1.4\times 10^2$	$7.9\times 10^2$	$8.7\times 10^2$	$5.4\times 10^{-1}$	$8.0\times 10^2$	$6.6\times 10^3$
FCC-eh	initial	$1.0\times 10^4$	$2.6\times 10^6$	$8.7\times 10^5$	$4.9\times 10^6$	$2.8\times 10^2$	$6.2\times 10^6$	$4.9\times 10^6$
	(i)	$1.1\times 10^3$	$4.5\times 10^3$	$4.0\times 10^4$	$3.8\times 10^4$	15	$1.3\times 10^4$	$2.8\times 10^5$
	(ii)	$8.7\times 10^2$	$1.5\times 10^3$	$1.9\times 10^4$	$1.7\times 10^4$	12	$4.1\times 10^3$	$1.2\times 10^5$

**Table 4:** The number of events for the signal with benchmark  $m_N = 120$  GeV and  $|V_{\tau N}|^2 |V_{eN}|^2 / (|V_{\tau N}|^2 + |V_{eN}|^2) = 5 \times 10^{-5}$ , and for six dominant background processes after applying preselection (i)-(ii) sequentially for the leptonic  $\tau_\mu$  final state. The numbers correspond to the LHeC and FCC-eh with 1 and 3  $\text{ab}^{-1}$  integrated luminosity, respectively.

To further reject the background, we input following nineteen observables to perform the BDT-MVA.

- A. Four momenta of the final state  $\tau_\mu$ :  $p_x(\tau_\mu), p_y(\tau_\mu), p_z(\tau_\mu), E(\tau_\mu)$ .
- B. Four momenta of the first three final state regular jets:  $p_x(j_1), p_y(j_1), p_z(j_1), E(j_1)$ ;  $p_x(j_2), p_y(j_2), p_z(j_2), E(j_2)$ ;  $p_x(j_3), p_y(j_3), p_z(j_3), E(j_3)$ .
- C. Number of regular jets:  $N(j)$ .

D. Magnitude and azimuthal angle of the missing transverse momentum:  $\cancel{E}_T, \phi(\cancel{E}_T)$ .

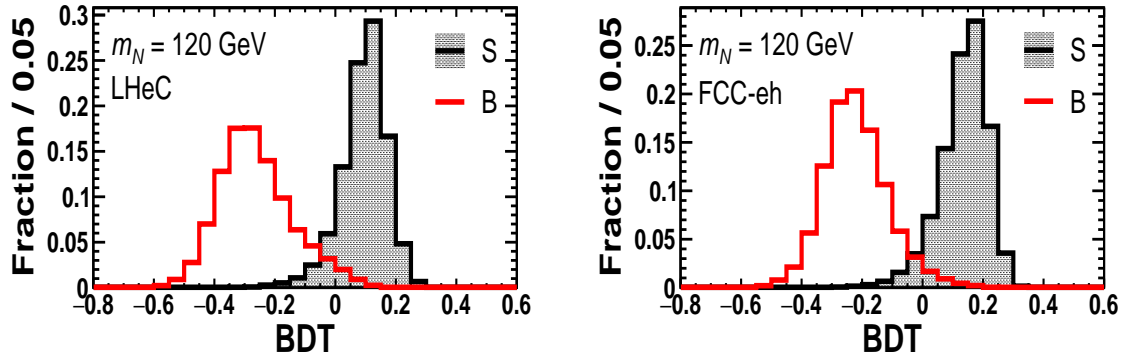


**Figure 5:** Distributions of BDT responses for the signal with benchmark  $m_N = 120$  GeV and  $|V_{\tau N}|^2 |V_{eN}|^2 / (|V_{\tau N}|^2 + |V_{eN}|^2) = 5 \times 10^{-5}$  (black, filled) and for total SM background (red) at the LHeC (left) and FCC-eh (right) for the leptonic  $\tau_\mu$  final state.

In Fig. 5, we show BDT distributions for the total background and the benchmark signal with  $m_N = 120$  GeV at the LHeC and FCC-eh. Since the kinematics of signal varies with  $m_N$ , distributions of BDT response also change with  $m_N$ . BDT distributions corresponding to other representative heavy neutrino masses are shown in Appendix B.2 for the LHeC and FCC-eh.

## 5 Results

In this section, based on our former analyses, we show the discovery sensitivities on the parameter  $|V_{\tau N}|^2 |V_{eN}|^2 / (|V_{\tau N}|^2 + |V_{eN}|^2)$  for the heavy neutrino mass  $m_N$  in the range of 10 to 3000 GeV. We also develop the strategy to reconstruct the heavy neutrino mass. Considering the heavy neutrino decays into one tau plus two jets for our signal, when  $m_N$  is above  $W$ -boson mass, we check di-jet combinations for all jets with  $p_T > 10$  GeV, and recognize the combination with its invariant mass closest to  $W$ -boson mass as the di-jet ( $j+j$ ) from the  $N$  decay. This di-jet is then combined with final state  $\tau_h$  ( $\tau_\mu$ ) and missing energy to reconstructed transverse mass  $M_T$  of the whole ( $\tau_h + j + j + \cancel{E}_T$ ) ( $(\tau_\mu + j + j + \cancel{E}_T)$ ) system. Here, transverse mass  $M_T \equiv \sqrt{(E_T^{\text{vis.}} + \cancel{E}_T)^2 - (\vec{p}_T^{\text{vis.}} + \vec{\cancel{p}}_T)^2}$ , where  $E_T^{\text{vis.}}$  ( $\vec{p}_T^{\text{vis.}}$ ) is the transverse energy (momentum) of the visible object or system,  $\cancel{E}_T$  ( $\vec{\cancel{p}}_T$ ) is the missing transverse energy (momentum).  $E_T^{\text{vis.}} = \sqrt{(\vec{p}_T^{\text{vis.}})^2 + (m^{\text{vis.}})^2}$ , where  $m^{\text{vis.}}$  is the invariant mass of the visible object or system.  $\cancel{E}_T = |\vec{\cancel{p}}_T|$ , assuming the invariant mass of the invisible object is zero. Fig 6 shows distributions of  $M_T(\tau_h + j + j + \cancel{E}_T)$  and  $M_T(\tau_\mu + j + j + \cancel{E}_T)$  for the signal with benchmark  $m_N = 120$  GeV after preselection at the LHeC and FCC-eh for the hadronic  $\tau_h$  (left) and leptonic  $\tau_\mu$  (right) final states, respectively. One observes that the transverse mass has sharp peak around  $m_N$ , which means that it can be used to reconstruct the heavy neutrino mass.

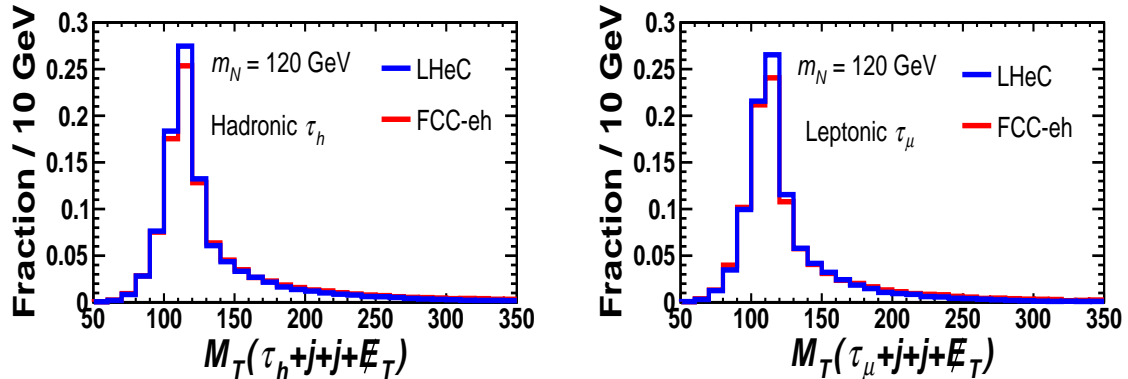


**Figure 6:** Distributions of transverse mass  $M_T$  of the  $(\tau + j + j + \cancel{E}_T)$  system for the signal with benchmark  $m_N = 120$  GeV and  $|V_{\tau N}|^2 |V_{eN}|^2 / (|V_{\tau N}|^2 + |V_{eN}|^2) = 5 \times 10^{-5}$  for the hadronic  $\tau_h$  (left) and leptonic  $\tau_\mu$  (right) final states, respectively.

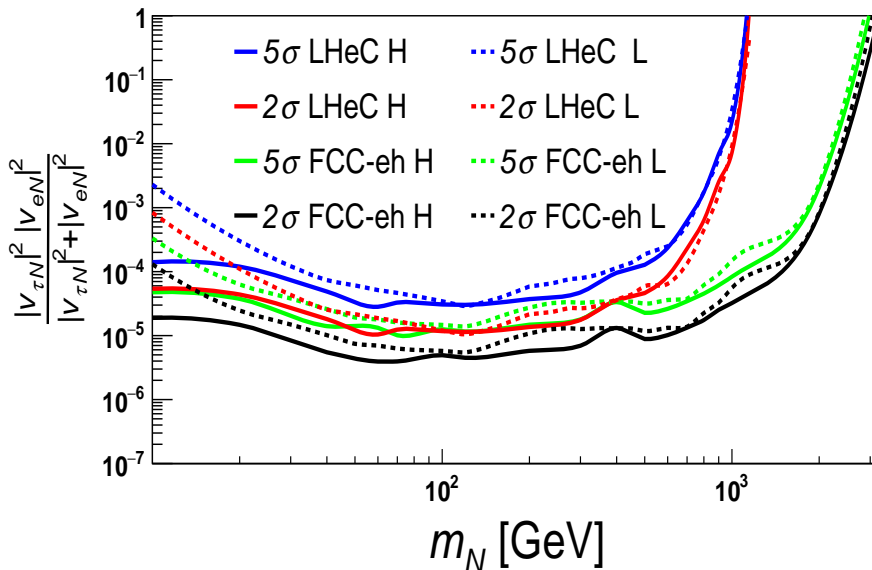
We note that above input observables listed in Sec. 3.2 and Sec. 4.2 including the four-momenta and angles are very basic and usually called low-level variables for the MVA. One can also construct some complicated observables and input such high-level variables to perform the MVA analysis. The BDT-MVA combines the information from all input observables with correlations. Because the low-level observables have already included the information of all final state objects, inputting the high-level observables will give similar BDT distributions and will not improve the final sensitivities a lot, c.f. Ref. [45]. However, distributions of high-level observables are helpful for researchers to understand the kinematics of both signal and background. They are usually more distinct between the signal and background, and can be used to perform the cut-based analysis. Therefore, in Appendix C, we show distributions of some high-level observables after preselection for the signal and dominant background processes assuming  $m_N = 120$  GeV for the hadronic  $\tau_h$  and leptonic  $\tau_\mu$  final states at the LHeC and FCC-eh, respectively.

After the preselection, the BDT selection is optimized according to the signal statistical significance calculated by Eq. (5.1) [100–102] for each mass case.

$$\sigma_{\text{stat}} = \sqrt{2 \left[ (N_s + N_b) \ln \left( 1 + \frac{N_s}{N_b} \right) - N_s \right]}, \quad (5.1)$$

where  $N_s$  ( $N_b$ ) is the number of signal (total background) events after all selections.

In Table 5, we show selection efficiencies of preselection and BDT requirements. for both the signal with representative  $m_N$  assumptions and background processes at the LHeC and FCC-eh for the hadronic  $\tau_h$  final state. Selection efficiencies for the leptonic  $\tau_\mu$  final state are shown in Table 6. The total selection efficiency is the product of preselection and BDT selection efficiencies. The number of signal or background events after all selections can be calculated by multiplying the production cross section, collider luminosity and total selection efficiency.



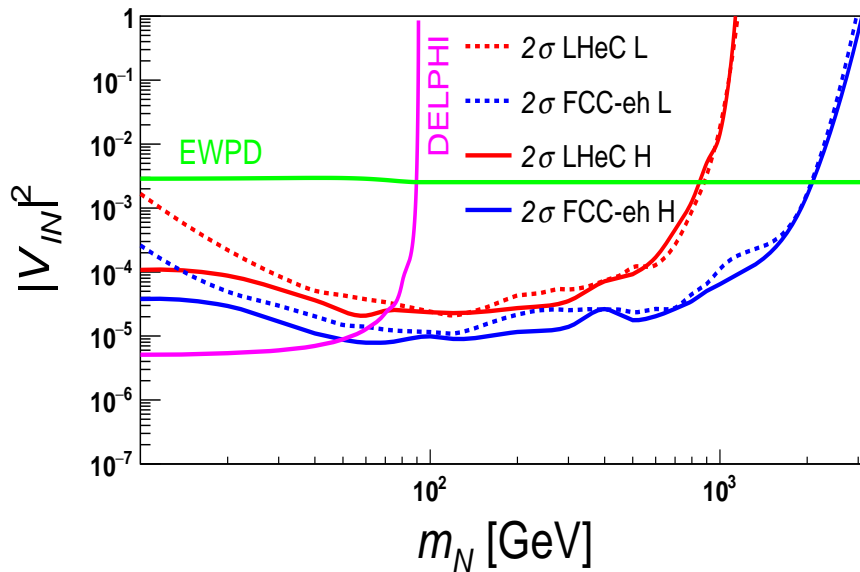
**Figure 7:** 2- and 5- $\sigma$  discovery sensitivities on the parameter  $|V_{\tau N}|^2 |V_{eN}|^2 / (|V_{\tau N}|^2 + |V_{eN}|^2)$  as varying the heavy neutrino mass in the range of 10 to 3000 GeV for the hadronic  $\tau_h$  (H) and leptonic  $\tau_\mu$  (L) final states at the LHeC and FCC-eh.

Fig. 7 presents discovery sensitivities at the 2- and 5- $\sigma$  significances on the parameter  $|V_{\tau N}|^2 |V_{eN}|^2 / (|V_{\tau N}|^2 + |V_{eN}|^2)$  for the heavy neutrino mass in the range of 10 to 3000 GeV. Both sensitivities for the hadronic  $\tau_h$  and leptonic  $\tau_\mu$  final states at the LHeC and FCC-eh are shown. At the LHeC, as  $m_N$  changes from 10 GeV to 120 GeV, for the leptonic  $\tau_\mu$  final state, the 2- $\sigma$  discovery sensitivities on  $|V_{\tau N}|^2 |V_{eN}|^2 / (|V_{\tau N}|^2 + |V_{eN}|^2)$  decrease from  $8.4 \times 10^{-4}$  to  $1.0 \times 10^{-5}$ , then begin to increase afterwards. The 2- $\sigma$  discovery sensitivity at the FCC-eh has similar behavior as that at the LHeC, but its varying range is much smaller, i.e., between  $1.3 \times 10^{-4}$  and  $5.4 \times 10^{-6}$ . At both colliders, the 5- $\sigma$  discovery sensitivities are slightly weaker than those for 2- $\sigma$ .

For the hadronic  $\tau_h$  final state, at the LHeC, as  $m_N$  changes from 10 GeV to 100 GeV, the 2- $\sigma$  discovery sensitivities on  $|V_{\tau N}|^2 |V_{eN}|^2 / (|V_{\tau N}|^2 + |V_{eN}|^2)$  decrease from  $5.4 \times 10^{-5}$  to  $1.2 \times 10^{-5}$ , then begin to increase afterwards. The 2- $\sigma$  discovery sensitivity at the FCC-eh also has similar behavior as that at the LHeC, but its varying range is smaller, i.e. between  $1.9 \times 10^{-5}$  and  $5.0 \times 10^{-6}$ . Compared with the leptonic  $\tau_\mu$  final state, the hadronic  $\tau_h$  final state has bigger signal rate due to larger branching ratio for hadronic tau decay mode, but it suffers from the misidentified tau background which restricts its discovery sensitivities. Therefore, sensitivities for both final states are found to be similar for most of the parameter space investigated in this study.

## 6 Sensitivities compared with current experimental limits

In Fig. 8, assuming mixing parameters  $|V_{\tau N}|^2 = |V_{eN}|^2 = |V_{\ell N}|^2$ , the  $2\text{-}\sigma$  discovery sensitivities on  $|V_{\ell N}|^2$  are shown for both the hadronic  $\tau_h$  and leptonic  $\tau_\mu$  final states at the LHeC and FCC-eh. With the same assumption, we also derive the limits on  $|V_{\ell N}|^2$  from Electroweak Precision Data (EWPD) [47–51, 53] and DELPHI experiment [46], and show them in the same plot for the comparison. The details of derivation process are shown in Appendix A. We observe that sensitivity bounds from the LHeC and FCC-eh are stronger than those from EWPD when  $m_N \lesssim 900$  GeV, and also stronger than those from DELPHI when  $m_N \gtrsim 70$  GeV.



**Figure 8:** Assuming the mixing parameter  $|V_{\ell N}|^2 = |V_{\tau N}|^2 = |V_{eN}|^2$ , the discovery sensitivities on  $|V_{\ell N}|^2$  at  $2\text{-}\sigma$  significance as the heavy neutrino mass changes from 10 to 3000 GeV for Hadronic  $\tau_h$  (H) and Leptonic  $\tau_\mu$  (L) final states at the LHeC and FCC-eh. The constraints from EWPD [47–51, 53] (green solid line) and DELPHI experiments [46] (purple solid line) are derived and displayed in the same plot for the comparison, see more details in Appendix A.

In this study, we require mixing parameters  $|V_{\tau N}|^2, |V_{eN}|^2 \neq 0$  and  $|V_{\mu N}|^2 = 0$ , and set discovery sensitivities on the parameter  $|V_{eN}|^2|V_{\tau N}|^2 / (|V_{eN}|^2 + |V_{\tau N}|^2)$ , which is a function of both  $|V_{\tau N}|^2$  and  $|V_{eN}|^2$ . Because of the challenges in detecting the final state taus, current experimental limits on mixing parameter  $|V_{\tau N}|^2$  are much weaker than those on  $|V_{eN}|^2$  and  $|V_{\mu N}|^2$ . Therefore, it is interesting to investigate the individual sensitivities on  $|V_{\tau N}|^2$ .

In Fig. 9, assuming representative heavy neutrino masses, we show the expected  $2\text{-}\sigma$  discovery sensitivities at future LHeC and FCC-eh colliders in the  $|V_{\tau N}|^2$  vs.  $|V_{eN}|^2$  plane, together with existed limits as a comparison. For any given mass, the expected  $2\text{-}\sigma$  discovery sensitivity for  $|V_{eN}|^2|V_{\tau N}|^2 / (|V_{eN}|^2 + |V_{\tau N}|^2)$  is a fixed number (as shown in Fig. 7), which

behaves as a hyperbola curve in the  $|V_{\tau N}|^2$  vs.  $|V_{eN}|^2$  plane. The top right parameter space of the curves is excluded. From Appendix A, yellow regions in all plots are allowed by the EWPD [47–51, 53], while the cyan region in the top left plot is allowed by the DELPHI measurement [46]. Constraints on  $|V_{eN}|^2$  from the LHC experiments [36, 37, 39] are shown as black dotted line, which appears only in the top left plot, because this constraint is too weak for large  $m_N$ .

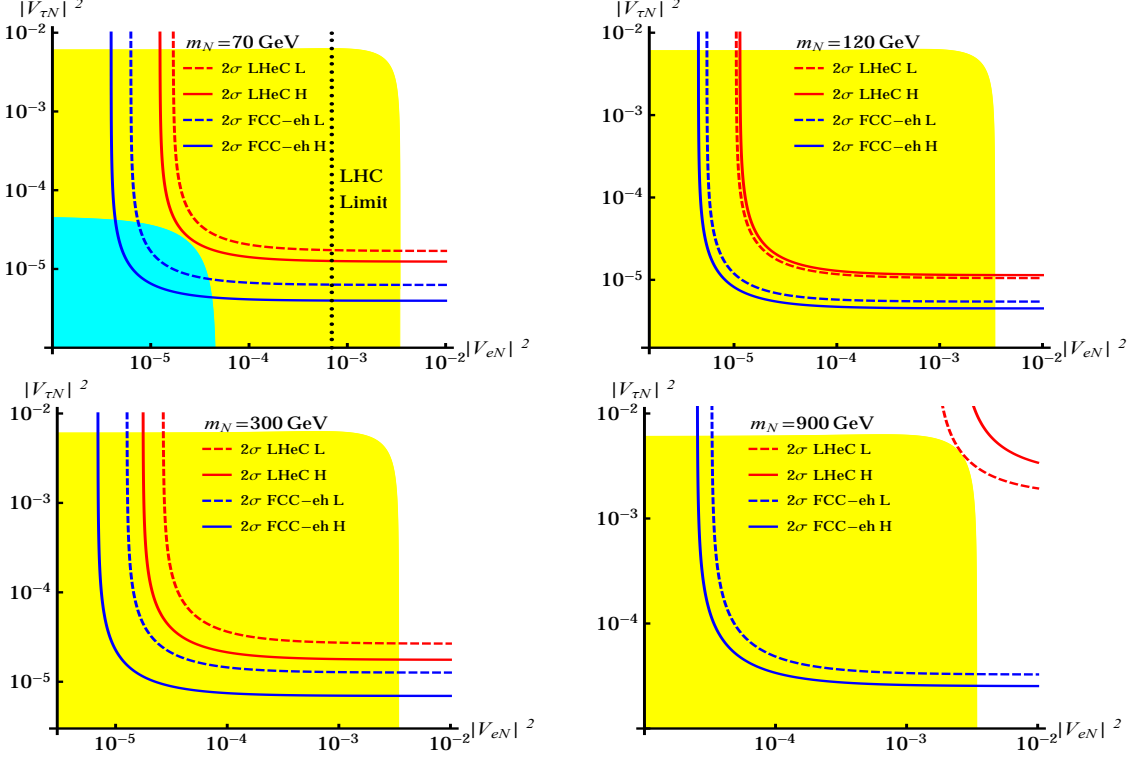


**Figure 9:** Assuming  $m_N = 70, 120, 300, 900$  GeV, the  $2\text{-}\sigma$  sensitivity curves for the Hadronic  $\tau_h$  (H, solid) and Leptonic  $\tau_\mu$  (L, dashed) final states at the LHeC (red) and FCC-eh (blue) in the  $|V_{\tau N}|^2$  vs.  $|V_{eN}|^2$  plane, where the top right parameter space of the curves are excluded. From Appendix A, yellow regions in all plots are allowed by the EWPD [47–51, 53], while the cyan region in the top left plot is allowed by the DELPHI measurement [46]. Constraints on  $|V_{eN}|^2$  from the LHC experiments [36, 37, 39] are shown as black dotted line, which appears only in the top left plot, because these constraints are too weak for large  $m_N$ .

In the top left plot, we choose  $m_N = 70$  GeV as a typical benchmark point when  $m_N < m_Z$ . In this case, results show that the future FCC-eh (both leptonic  $\tau_\mu$  and hadronic  $\tau_h$  final states) and LHeC experiments (only hadronic  $\tau_h$  final state) are both possible to probe additional parameter space compared with the DELPHI experiment. In other three plots, we choose  $m_N = 120, 300,$  and  $900$  GeV as benchmark points, and all of them locate in the range where  $m_N > m_Z$ . In these cases, the combination of measurements from EWPD

and searches at  $pe$  collider constrain the parameter space synergistically, while the limits on  $|V_{eN}|^2$  from the LHC experiments are much weaker and not shown. Our results show that except at very large  $m_N$  region, for example,  $m_N \gtrsim 900$  GeV, the expected sensitivity from LHeC experiment will be similar to that from EWPD, due to the quickly decreasing signal production cross section. For other mass ranges, future LHeC and FCC-eh experiments are expected to significantly enhance the discovery potential for a large portion of the  $|V_{\tau N}|^2$  vs.  $|V_{eN}|^2$  plane, compared with the EWPD and LHC searches.

## 7 Conclusion and discussion

In this paper, we utilize the lepton number violation signal process of  $pe^- \rightarrow \tau^+ jjj$  to search for heavy Majorana neutrinos at the future electron-proton colliders. We consider the LHeC (FCC-eh) running with an electron beam energy of 60 GeV, a proton beam energy of 7 (50) TeV and an integrated luminosity of 1 (3)  $\text{ab}^{-1}$ . The electron beam is considered to be unpolarized. To simplify the analyses, we consider the phenomenological simplified Type-I and assume that only one generation of heavy neutrinos  $N$  is within the collider access and mixes with active neutrinos of tau and electron flavours, i.e.  $|V_{\tau N}|^2, |V_{eN}|^2 \neq 0$  and  $|V_{\mu N}|^2 = 0$ . We perform analyses for both hadronic  $\tau_h$  and leptonic  $\tau_\mu$  final states, and forecast discovery sensitivities for heavy neutrinos mass  $m_N$  in the range 10-3000 GeV at LHeC and FCC-eh.

The cross sections of the LNV signal  $pe^- \rightarrow \tau^+ jjj$  are presented in Fig. 2 as a function of  $m_N$  at the LHeC and FCC-eh. We apply detector configurations and simulate signal and related SM background events for both hadronic  $\tau_h$  and leptonic  $\tau_\mu$  final states. When tau decays hadronically (leptonically), we select the final state containing the tau-jet (muon). The preselections are applied to select the signal and reject the background events at the first stage. Then various observables are input, and the BDT algorithm is adopted to perform the multivariate analysis and maximally reject the background. The BDT distributions with different  $m_N$  assumptions are presented and some high-level observables corresponding benchmark  $m_N$  case are shown in appendices.

The strategy to reconstruct the heavy neutrino mass is developed and distributions of reconstructed mass are presented. After the preselection, the BDT selection is optimized to maximize the signal statistical significance. In Appendix D, we show selection efficiencies of preselection and BDT requirements. for both the signal with representative  $m_N$  assumptions and background processes at the LHeC and FCC-eh. The discovery sensitivities on parameter  $|V_{\tau N}|^2 |V_{eN}|^2 / (|V_{\tau N}|^2 + |V_{eN}|^2)$  for the heavy neutrino mass in the range of 10 to 3000 GeV are presented in Fig. 7. At the  $2\text{-}\sigma$  significance, the best sensitivity is  $\sim 1.2 \times 10^{-5}$  ( $5.0 \times 10^{-6}$ ) at the LHeC (FCC-eh) when  $m_N \sim 100$  GeV for the hadronic  $\tau_h$  final state. The discovery sensitivities for the leptonic  $\tau_\mu$  final state are found to be similar for most of the parameter space investigated than those for the hadronic  $\tau_h$  final state.

We derive the limits on the mixing parameters from EWPD and DELPHI experiment in Appendix A. Assuming  $|V_{\tau N}|^2 = |V_{eN}|^2 = |V_{\ell N}|^2$ , sensitivities on  $|V_{\ell N}|^2$  from  $pe$  collider



searches are compared with those from the EWPd and DELPHI experiment in Fig. 8. We find that sensitivity bounds from the LHeC and FCC-eh are stronger than those from EWPd for almost all the mass range, and also stronger than those from DELPHI when  $m_N \gtrsim 70$  GeV.

To investigate the individual sensitivities on  $|V_{\tau N}|^2$ , in Fig. 9, assuming representative  $m_N$ , we show the expected 2- $\sigma$  sensitivity curves from  $pe$  collider searches in the  $|V_{\tau N}|^2$  vs.  $|V_{eN}|^2$  plane, together with existed limits from EWPd, DELPHI, and LHC experiments for comparison. Our results show that compared with current experimental limits, future  $pe$  experiments can probe large additional regions in the parameter space formed by  $|V_{\tau N}|^2$  and  $|V_{eN}|^2$ , and thus significantly enhance the discovery potential for a large portion of the  $|V_{\tau N}|^2$  vs.  $|V_{eN}|^2$  plane.

Compared our sensitivity results with those in Ref [45], at  $pe$  colliders, sensitivities for the  $\tau^+$  final state are weaker than the  $\mu^+$  final state. This is mainly because that (i) due to the challenges in detecting the final state taus, the signal rate is much lower for the  $\tau^+$  final state; (ii) the  $\tau^+$  final state also suffers from larger background. Besides, as pointed in Ref [45], because the total background cross section for the  $e^+$  final state is about three times larger than that for the  $\mu^+$  final state, sensitivities for the  $e^+$  final state is expected to be weaker than those for the  $\mu^+$  final state. However, because the  $pe^- \rightarrow e^+jjj$  signal process can depend on the mixing parameter  $|V_{eN}|^2$  only, it is a unique channel to probe  $|V_{eN}|^2$  independent of other mixing parameters. In this sense, the detailed analyses of the  $e^+$  final state are still meaningful, and we leave it for future studies.

A jet can be misidentified as a hadronic  $\tau_h$  in the detector, which can contribute to the background for the hadronic  $\tau_h$  final state. Because of the huge production cross section, even a small misidentification rate of jet to hadronic tau can still lead to large background. To estimate its effects, we include the multi-jet process “ $pe^- \rightarrow \nu_ejjj$ ” in the background. Our analysis indicates that the  $\Delta R(\tau, j)$  and BDT requirements can reject such background effectively. However, because this background is greatly affected by the detector’s performance and the detectors of future  $pe$  colliders are still under development, it should be carefully considered for future studies.

## A Constraints from $Z \rightarrow N\nu, N\bar{\nu}$ rare decay channels and EWPd

In this appendix, we show details about the constraints from  $Z$ -boson rare decay [46] and EWPd [47–51, 53]. In this paper, since we consider the signal process  $pe^- \rightarrow N(\rightarrow \tau^+W^-)j$  corresponding to both  $W$ - $N$ - $e$  and  $W$ - $N$ - $\tau$  vertices, thus we assume mixing parameters  $|V_{eN}|^2$  and  $|V_{\tau N}|^2$  are both nonzero. We also assume  $|V_{\mu N}|^2 = 0$  here for simplicity.

First, we consider the  $Z$ -boson rare decay processes. If  $m_N < m_Z$ , the two-body rare

decay channels  $Z \rightarrow N\nu, N\bar{\nu}$  are open <sup>1</sup> with the partial width

$$\frac{\Gamma_{Z \rightarrow N\nu_\ell}}{\Gamma_{Z \rightarrow \nu_\ell \bar{\nu}_\ell}} = \frac{\Gamma_{Z \rightarrow N\bar{\nu}_\ell}}{\Gamma_{Z \rightarrow \nu_\ell \bar{\nu}_\ell}} = |V_{\ell N}|^2 f\left(\frac{m_N}{m_Z}\right), \quad (\text{A.1})$$

with the function

$$f(x) \equiv \begin{cases} (1-x^2)^2(1+x^2/2), & (x \leq 1); \\ 0 & (x > 1). \end{cases} \quad (\text{A.2})$$

Finally, we obtain the branching ratio for exotic decay

$$\text{Br}_{\text{exo}} \simeq 0.13 (|V_{eN}|^2 + |V_{\tau N}|^2) f\left(\frac{m_N}{m_Z}\right). \quad (\text{A.3})$$

Experimentally,  $\text{Br}_{\text{exo}} \lesssim 1.3 \times 10^{-6}$  at 95% C.L. [46], and thus Eq. (A.3) corresponds to the upper limit

$$|V_{eN}|^2 + |V_{\tau N}|^2 \lesssim \frac{10^{-5}}{f(m_N/m_Z)} \quad (\text{A.4})$$

for  $m_N < m_Z$ . Assuming  $|V_{\tau N}|^2 = |V_{eN}|^2 = |V_{\ell N}|^2$ , we show the 95% C.L. upper limit on  $|V_{\ell N}|^2$  in Fig. 8 as a comparison with the expected future LHeC or FCC-eh sensitivities in the  $m_N < m_Z$  region.

When  $m_N > m_Z$ , the two body  $Z \rightarrow N\nu, N\bar{\nu}$  decay channels are closed and thus we need to find the constraints from EWPD. In the EWPD studies, the observables  $\alpha$ ,  $G_F$ , and  $m_Z$  which have the best accuracy are treated as inputs [103, 104]

$$\begin{aligned} m_Z &= 91.2 \text{ GeV}, & G_F &= 1.166 \times 10^{-5} \text{ GeV}^{-2}, \\ \alpha^{-1}(0) &= 137.0, & \alpha^{-1}(m_Z) &= 128.0. \end{aligned} \quad (\text{A.5})$$

Other observables are derived from  $\alpha$ ,  $G_F$ , and  $m_Z$ . For example, in the SM, we have the tree level relation <sup>2</sup>

$$s_W^2 c_W^2 = \frac{\pi \alpha}{\sqrt{2} G_F m_Z^2}. \quad (\text{A.6})$$

The weak coupling is denoted as  $G_W \equiv \frac{g^2}{4\sqrt{2}m_W^2}$ , and is equivalent to the Fermi constant  $G_F$  in the SM. However, experimentally the Fermi constant  $G_F$  is extracted from the  $\mu \rightarrow e\nu_e\bar{\nu}_\mu$  decay process, which should be modified from  $G_W$  by a nonzero  $|V_{eN}|^2$  as

$$G_F = G_W \sqrt{1 - |V_{eN}|^2} \simeq G_W \left(1 - \frac{|V_{eN}|^2}{2}\right). \quad (\text{A.7})$$

Based on Eq. (A.6), we have the modification of  $s_W^2$  comparing with its SM value as

$$\frac{s_W^2}{s_{W,\text{SM}}^2} - 1 = -\frac{c_{W,\text{SM}}^2}{2c_{2W,\text{SM}}^2} |V_{eN}|^2 = -0.714 |V_{eN}|^2. \quad (\text{A.8})$$

<sup>1</sup>If  $m_N < m_Z/2$ , the decay channel  $Z \rightarrow NN$  is also open. However, its partial decay width behaves as  $\Gamma_{Z \rightarrow NN} \propto |V_{\ell N}|^4$ , which is always ignorable comparing with the  $Z \rightarrow N\nu, N\bar{\nu}$  decay channels.

<sup>2</sup>Here  $\sin\theta_W$ ,  $\cos\theta_W$ , and  $\tan\theta_W$  are separately denoted as  $s_W$ ,  $c_W$ , and  $t_W$  for simplicity.

The partial decay widths of a  $Z$ -boson to fermion pairs should be

$$\Gamma_{Z \rightarrow f\bar{f}} = \frac{N_c G_W m_Z^3}{6\sqrt{2}\pi} (g_{V,f}^2 + g_{A,f}^2), \quad (\text{A.9})$$

where  $g_{V,f} = T_{3,f} - 2Q_f s_W^2$  and  $g_{A,f} = T_{3,f}$ . Thus the partial decay widths of  $Z$  to fermion pairs are also modified due to the modifications in  $G_W$  and  $s_W^2$  as following.

$$\frac{\Gamma_{Z \rightarrow \ell^+ \ell^-}}{\Gamma_{Z \rightarrow \ell^+ \ell^-, \text{SM}}} = \frac{G_W}{G_F} \left(1 + 0.101 |V_{eN}|^2\right); \quad (\text{A.10})$$

$$\frac{\Gamma_{Z \rightarrow \nu_e \bar{\nu}_e, \nu_\tau \bar{\nu}_\tau}}{\Gamma_{Z \rightarrow \nu_e \bar{\nu}_e, \nu_\tau \bar{\nu}_\tau, \text{SM}}} = \frac{G_W}{G_F} \left(1 - |V_{eN}, \tau N|^2\right)^2; \quad (\text{A.11})$$

$$\frac{\Gamma_{Z \rightarrow \nu_\mu \bar{\nu}_\mu}}{\Gamma_{Z \rightarrow \nu_\mu \bar{\nu}_\mu, \text{SM}}} = \frac{G_W}{G_F}; \quad (\text{A.12})$$

$$\frac{\Gamma_{Z \rightarrow u_i \bar{u}_i}}{\Gamma_{Z \rightarrow u_i \bar{u}_i, \text{SM}}} = \frac{G_W}{G_F} \left(1 + 0.294 |V_{eN}|^2\right); \quad (\text{A.13})$$

$$\frac{\Gamma_{Z \rightarrow d_i \bar{d}_i}}{\Gamma_{Z \rightarrow u_i \bar{u}_i, \text{SM}}} = \frac{G_W}{G_F} \left(1 + 0.206 |V_{eN}|^2\right); \quad (\text{A.14})$$

$$\frac{\Gamma_{Z \rightarrow \text{had}}}{\Gamma_{Z \rightarrow \text{had}, \text{SM}}} = \frac{G_W}{G_F} \left(1 + 0.235 |V_{eN}|^2\right). \quad (\text{A.15})$$

In above equations,  $\ell$  denotes charged leptons,  $\nu$  denotes neutrinos,  $u_i$  denotes up-type quarks,  $d_i$  denotes down-type quarks, and the index ‘‘had’’ denotes all hadrons. We then obtain the modification of the  $Z$ -boson total decay width as

$$\frac{\Gamma_Z}{\Gamma_{Z, \text{SM}}} = \frac{G_W}{G_F} \left[1 + 0.175 |V_{eN}|^2 - 0.133 \left(|V_{eN}|^2 + |V_{\tau N}|^2\right) \left(1 - f \left(\frac{m_N}{m_Z}\right)\right)\right]. \quad (\text{A.16})$$

If  $m_N > m_Z$ , Eq. (A.16) becomes

$$\frac{\Gamma_Z}{\Gamma_{Z, \text{SM}}} = 1 + 0.541 |V_{eN}|^2 - 0.133 |V_{\tau N}|^2. \quad (\text{A.17})$$

Some useful observables in EWPD study are defined as [103, 104]

$$\begin{aligned} R_\ell &\equiv \frac{\Gamma_{Z \rightarrow \text{had}}}{\Gamma_{Z \rightarrow \ell^+ \ell^-}}, \quad R_q \equiv \frac{\Gamma_{Z \rightarrow q\bar{q}}}{\Gamma_{Z \rightarrow \text{had}}}, \quad \text{and} \\ \sigma_H &\equiv \sigma_{e^+ e^- \rightarrow Z \rightarrow \text{had}} = \frac{12\pi \Gamma_{Z \rightarrow e^+ e^-} \Gamma_{Z \rightarrow \text{had}}}{m_Z^2 \Gamma_Z^2}. \end{aligned} \quad (\text{A.18})$$

The modifications of these quantities can be derived as

$$\frac{R_\ell}{R_{\ell, \text{SM}}} - 1 = 0.134 |V_{eN}|^2; \quad (\text{A.19})$$

$$\frac{R_c}{R_{c, \text{SM}}} - 1 = 0.059 |V_{eN}|^2; \quad (\text{A.20})$$

$$\frac{R_c}{R_{c, \text{SM}}} - 1 = -0.029 |V_{eN}|^2; \quad (\text{A.21})$$

$$\frac{\sigma_H}{\sigma_{H, \text{SM}}} - 1 = 0.267 \left(|V_{eN}|^2 + |V_{\tau N}|^2\right) \left(1 - f \left(\frac{m_N}{m_Z}\right)\right) - 0.013 |V_{eN}|^2. \quad (\text{A.22})$$

If  $m_N > m_Z$ , Eq. (A.22) becomes

$$\frac{\sigma_H}{\sigma_{H,\text{SM}}} - 1 = 0.254 |V_{eN}|^2 + 0.267 |V_{\tau N}|^2. \quad (\text{A.23})$$

We perform the global-fit using the observables  $R_{q=b,c}$ ,  $R_{\ell=e,\mu,\tau}$ ,  $\sigma_H$ ,  $\Gamma_Z$  [103, 104], and also  $s_W^2$  extracted from Tevatron [105] and LHC [106]. Assuming  $|V_{\tau N}|^2 = |V_{eN}|^2 = |V_{\ell N}|^2$ , we show the 95% C.L. upper limit on  $|V_{\ell N}|^2$  in Fig. 8 as a comparison with the expected future LHeC or FCC-eh sensitivities. It depends weakly on  $m_N$ , and in the  $m_N > m_Z$  region, the limit is about  $|V_{\ell N}|^2 \lesssim 2.5 \times 10^{-3}$ . Our results are consistent with those in [51, 53]<sup>3</sup>.

---

<sup>3</sup>Numerical study shows that the constraint from  $\tau \rightarrow e\gamma$  rare decay is always weaker than that from EWPD and  $Z \rightarrow N\nu, N\bar{\nu}$  rare decay in the whole  $m_N$  region, and thus we do not show it in our results.

## B Distributions of BDT responses

### B.1 Hadronic $\tau_h$ final state

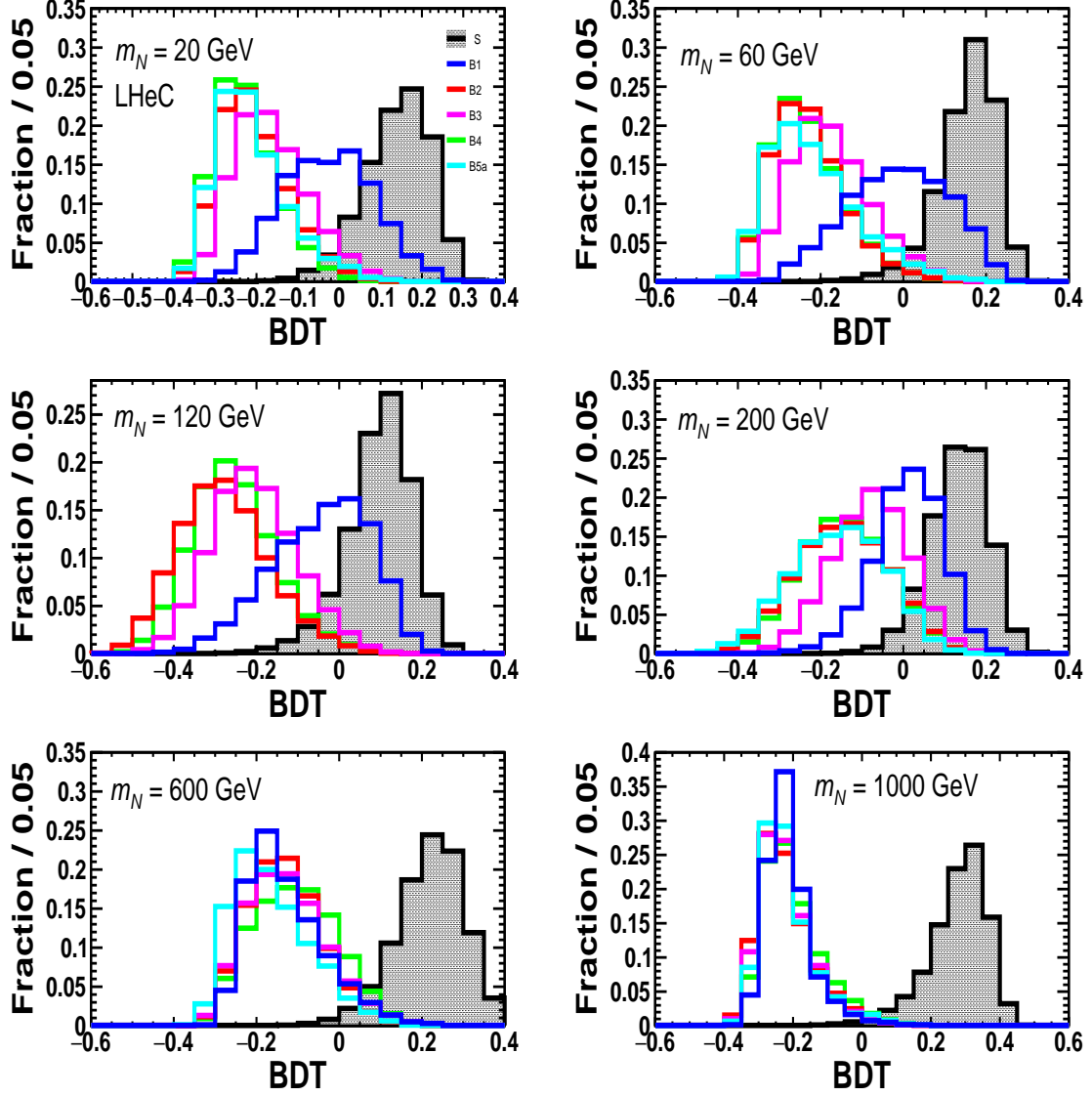


**Figure 10:** Distributions of BDT responses for the signal (black, filled) and background processes at the LHeC with different  $m_N$  assumptions and fixing  $|V_{\tau N}|^2 |V_{eN}|^2 / (|V_{\tau N}|^2 + |V_{eN}|^2) = 5 \times 10^{-5}$ , for the hadronic  $\tau_h$  final state.

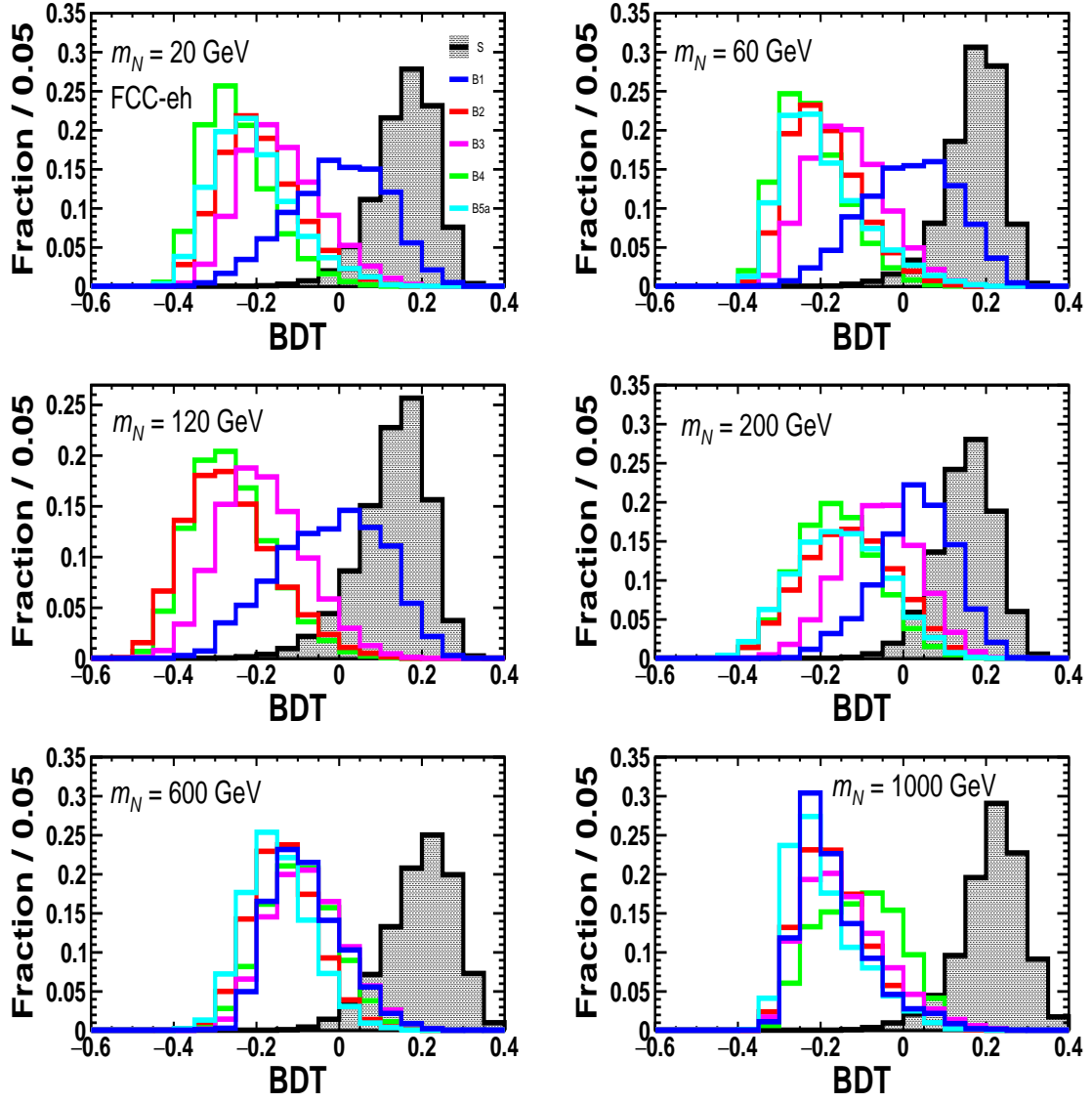
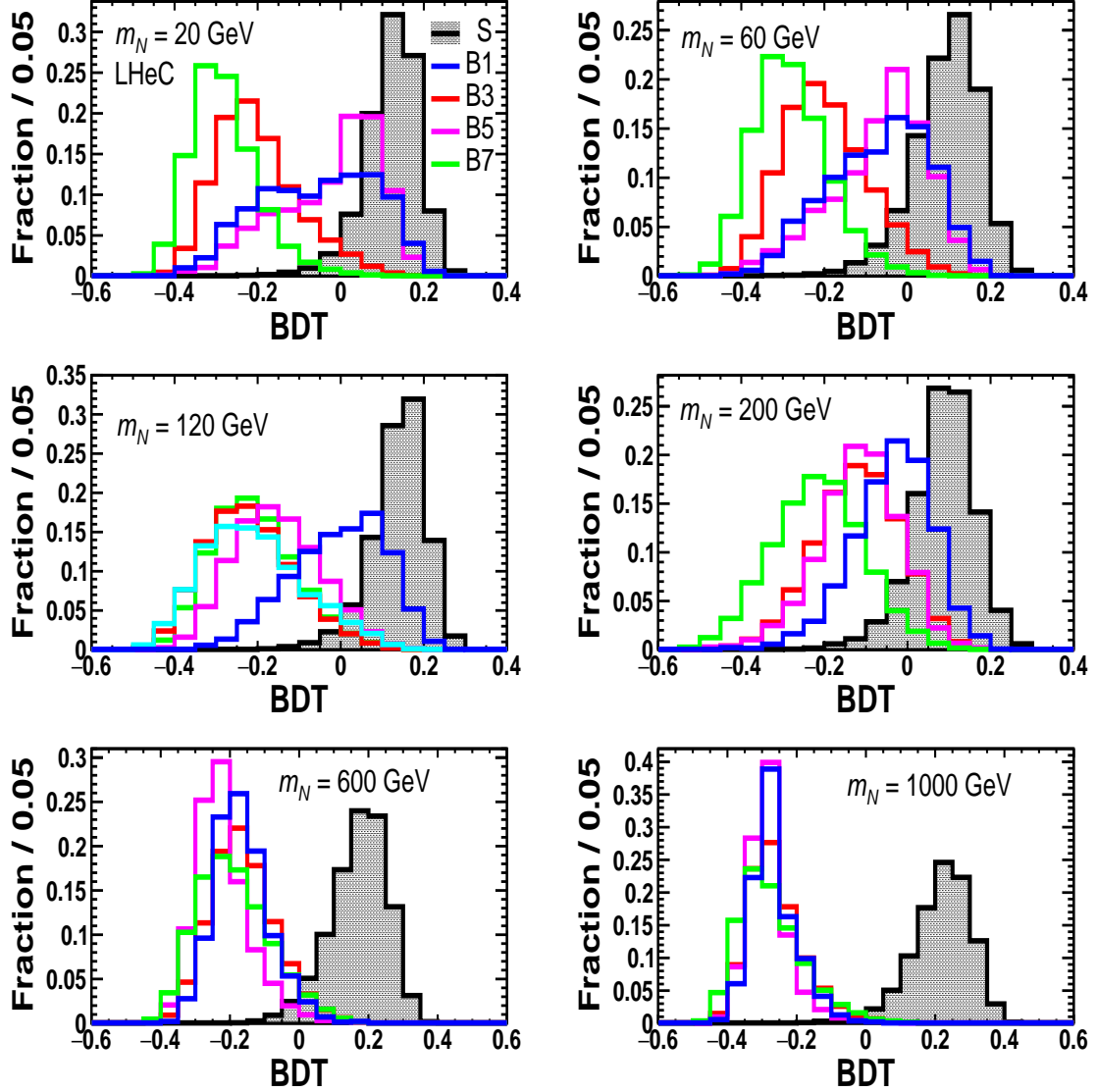


Figure 11: Similar as Fig. 10, but at the FCC-eh.

## B.2 Leptonic $\tau_\mu$ final state



**Figure 12:** Distributions of BDT responses for the signal (black, filled) and dominant background processes at the LHeC with different  $m_N$  assumptions and fixing  $|V_{\tau N}|^2 |V_{eN}|^2 / (|V_{\tau N}|^2 + |V_{eN}|^2) = 5 \times 10^{-5}$ , for the leptonic  $\tau_\mu$  final state.

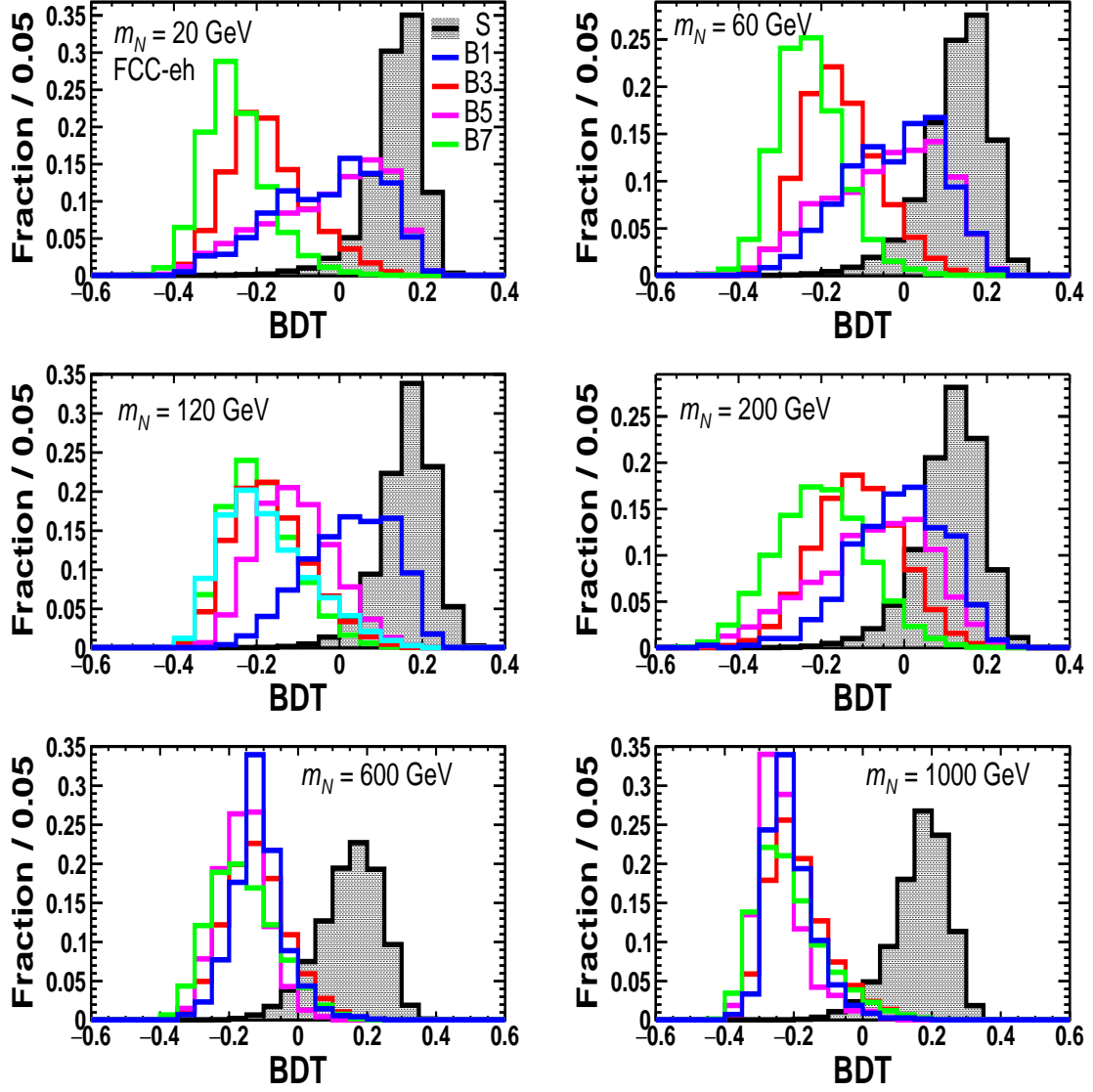


Figure 13: Similar as Fig. 12, but at the FCC-eh.



## C Distributions of representative high-level observables

Here,  $\cancel{E}_T$  is the magnitude of the missing transverse momentum.  $p_T$  and  $\eta$  are the transverse momentum and pseudorapidity of the final state object, respectively.  $\Delta\phi(\tau_h/\tau_\mu, \cancel{E}_T)$  is the azimuthal angle difference between the final state  $\tau_h / \tau_\mu$  and missing transverse momentum.  $M_T(\tau_h/\tau_\mu + \cancel{E}_T)$  is the transverse mass of the system of final state  $\tau_h / \tau_\mu$  and missing transverse momentum. The invariant mass of the di-jet  $M(j+j)$  denotes the reconstructed  $W$ -boson mass, and the transverse mass  $M_T(\tau_h/\tau_\mu + j+j + \cancel{E}_T)$  measures the reconstructed  $N$  mass, which are explained in Sec. 5.

### C.1 Hadronic $\tau_h$ final state

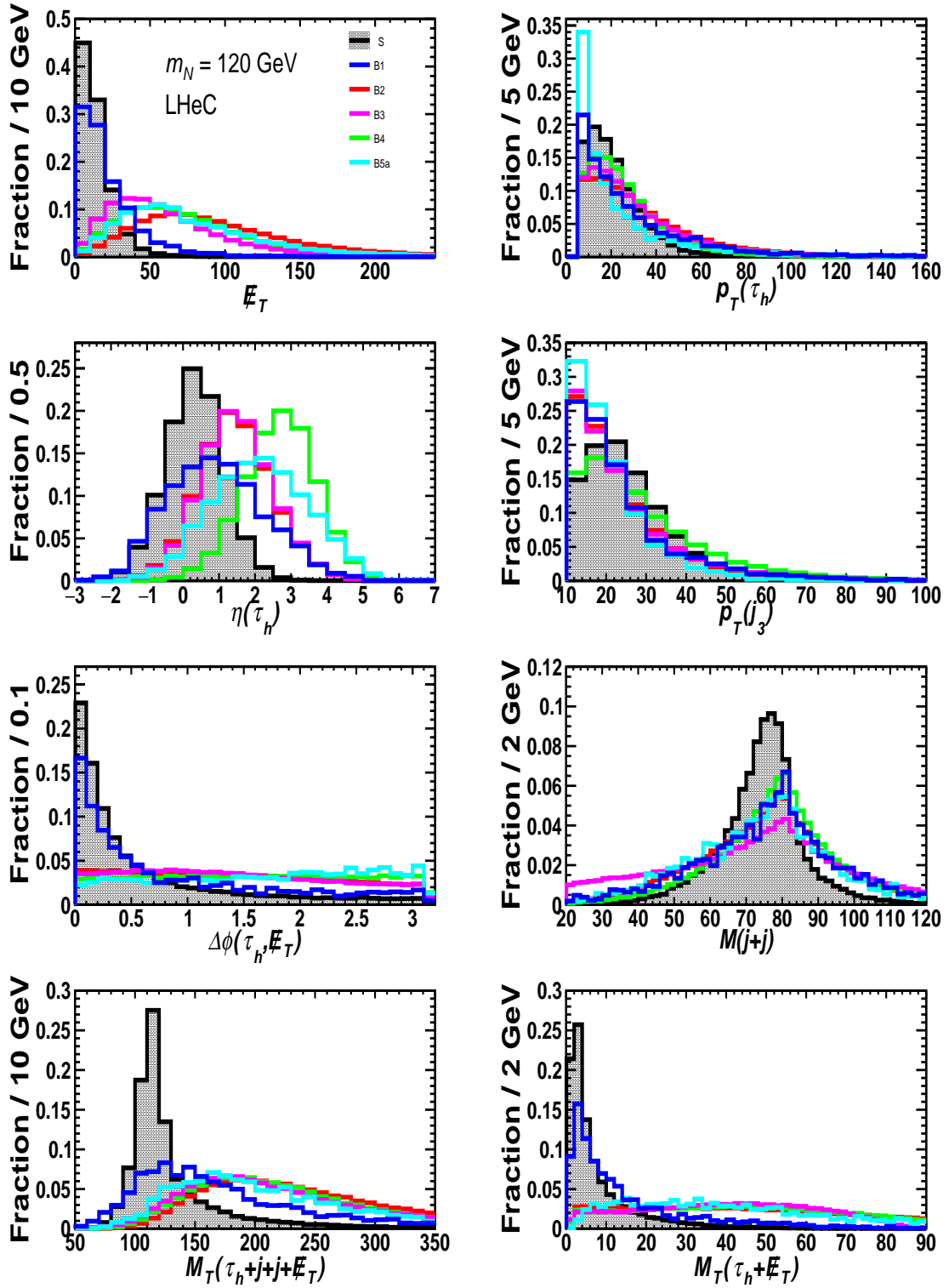


**Figure 14:** Distributions of some high-level observables after preselection for the signal (black, filled) and background processes at the LHeC assuming benchmark  $m_N = 120$  GeV and  $|V_{\tau N}|^2 |V_{eN}|^2 / (|V_{\tau N}|^2 + |V_{eN}|^2) = 5 \times 10^{-5}$ , for the hadronic  $\tau_h$  final state.

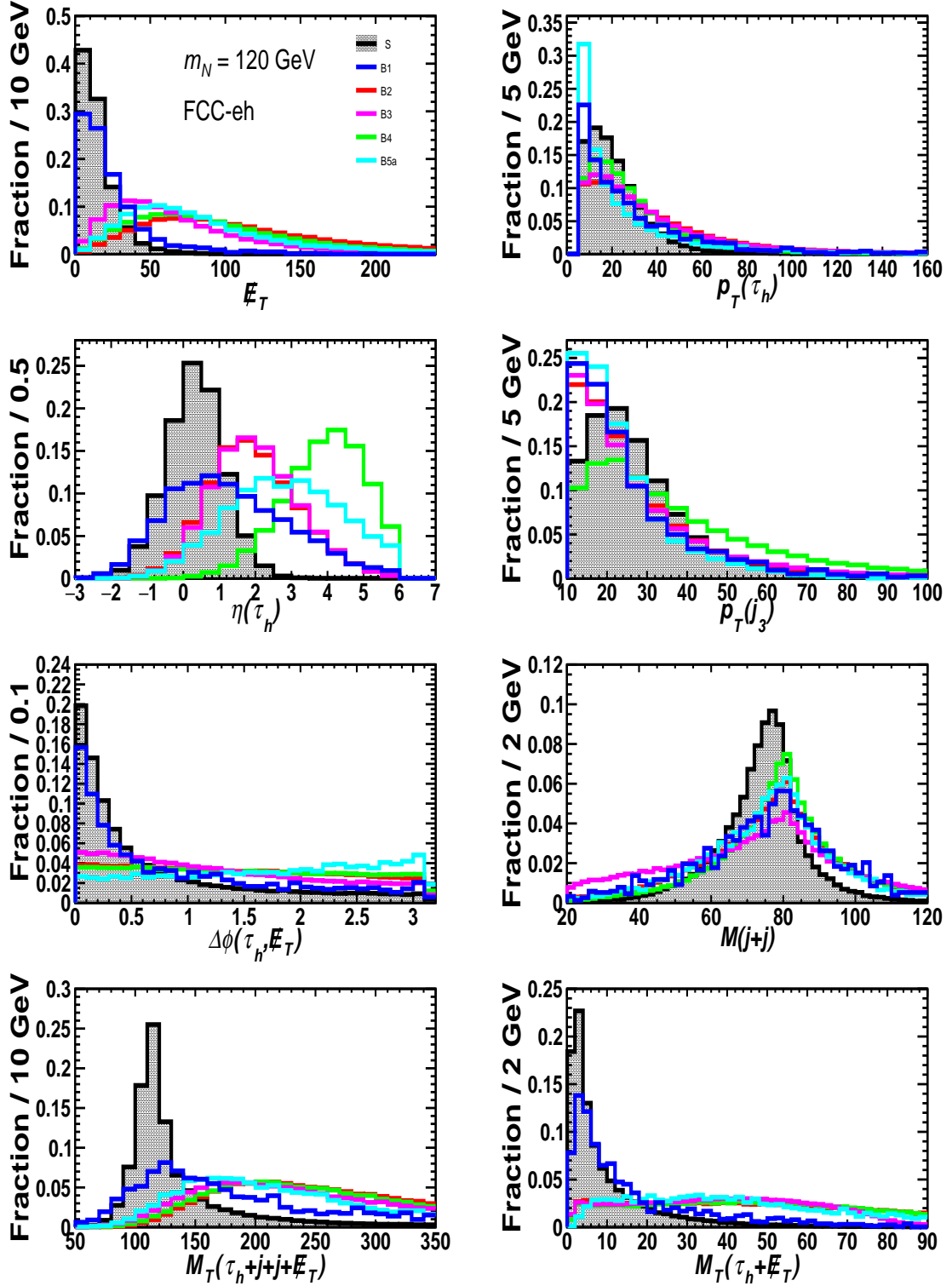
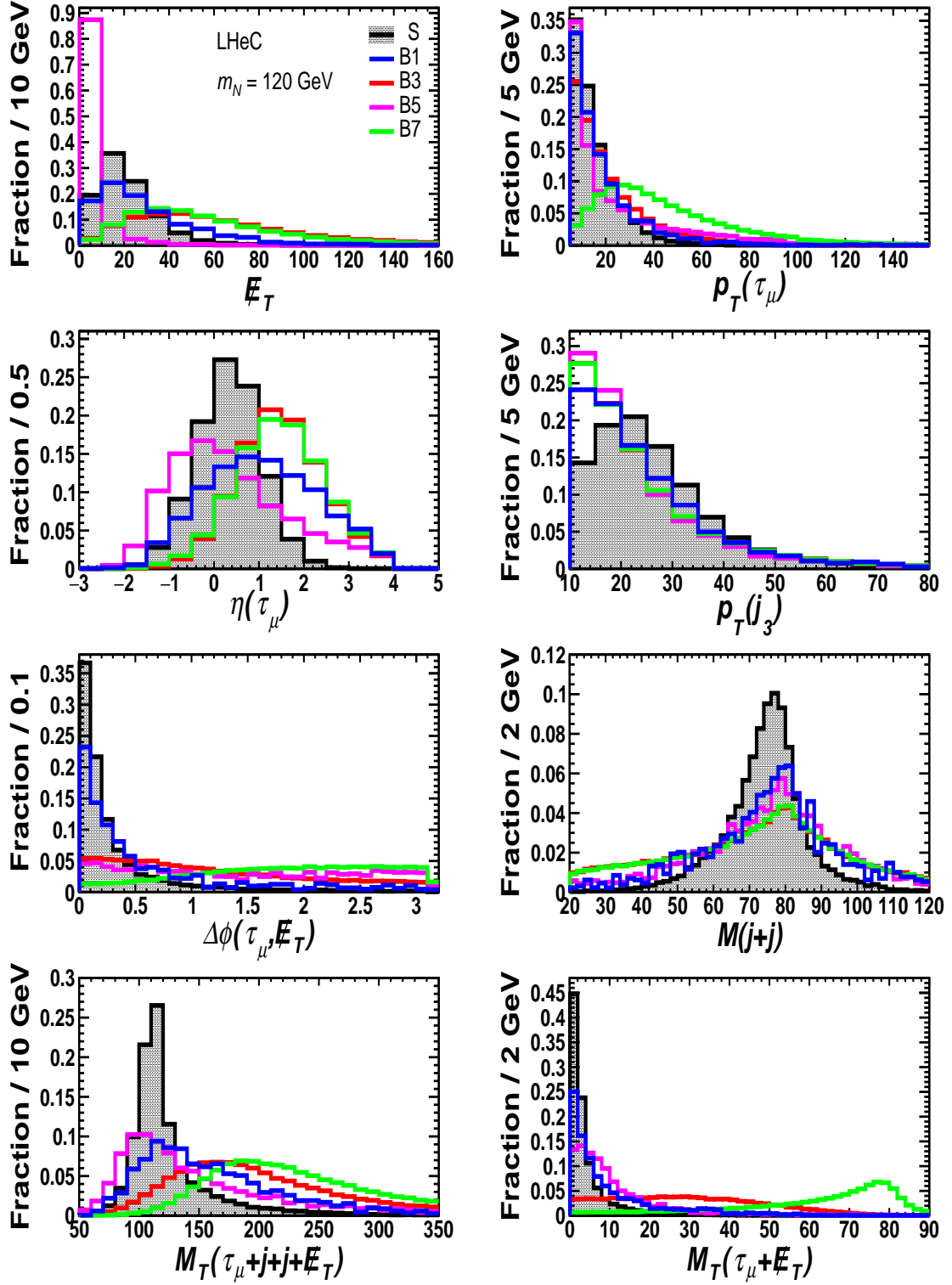


Figure 15: Similar as Fig. 14, but at the FCC-eh.

## C.2 Leptonic $\tau_\mu$ final state



**Figure 16:** Distributions of some high-level observables after preselection for the signal (black, filled) and dominant background processes at the LHeC assuming benchmark  $m_N = 120$  GeV and  $|V_{\tau N}|^2 |V_{eN}|^2 / (|V_{\tau N}|^2 + |V_{eN}|^2) = 5 \times 10^{-5}$ , for the leptonic  $\tau_\mu$  final state.

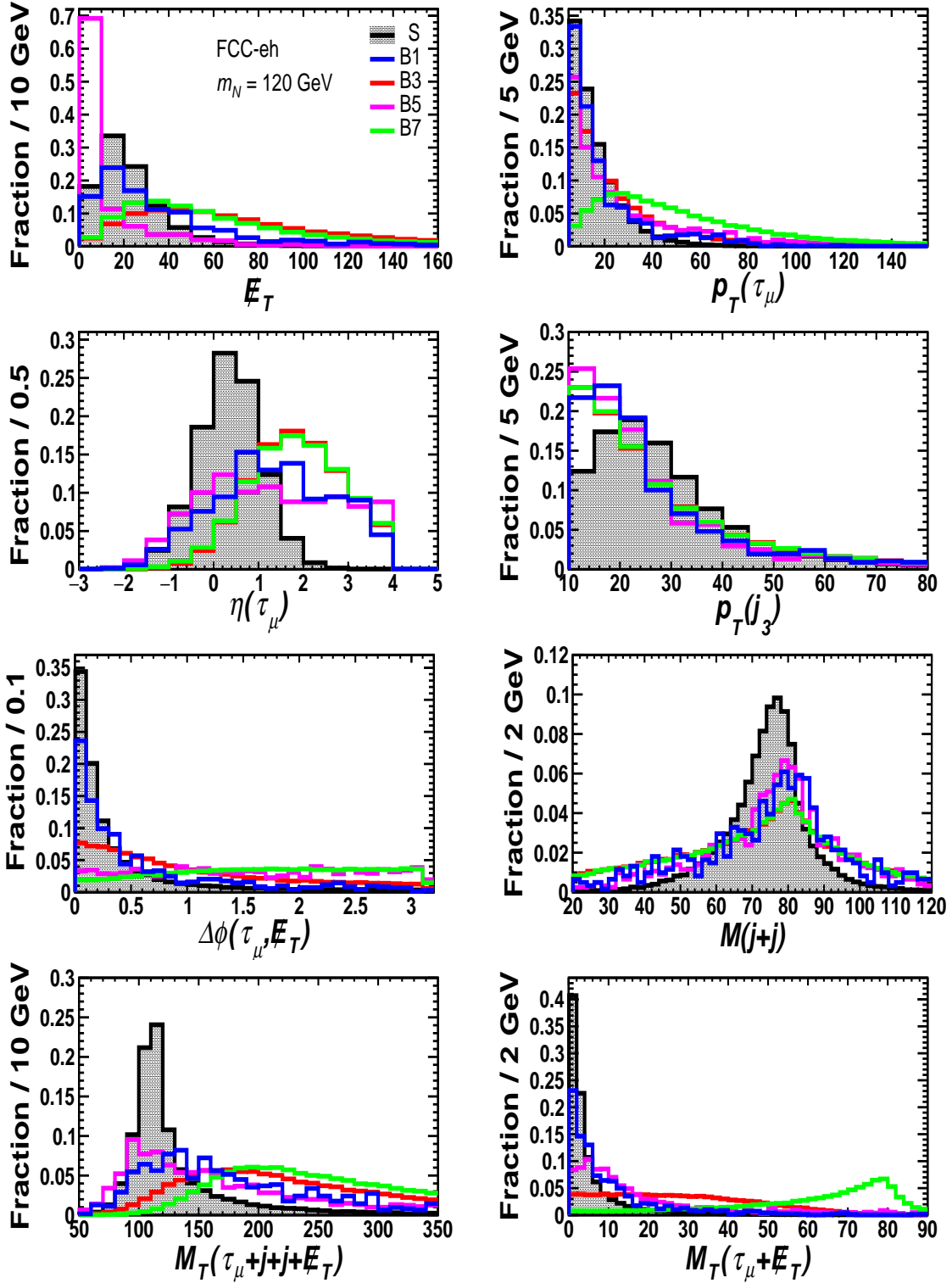


Figure 17: Similar as Fig. 16, but at the FCC-eh.

## D The Selection efficiency tables

### D.1 Hadronic $\tau_h$ final state

$m_N$	collider	selection	signal	$\tau^+\tau^-e^-jjj$	$\tau^+\tau^-\nu_ejjj$	$\tau^+\nu_\tau e^-jjj$	$\tau^+\nu_\tau\nu_ejjj$	$\nu_ejjjj$
20 GeV	LHeC	preselection	$1.19\times 10^{-2}$	$2.17\times 10^{-3}$	$3.22\times 10^{-2}$	$6.78\times 10^{-3}$	$1.48\times 10^{-1}$	$2.14\times 10^{-4}$
		BDT>0.184	$3.17\times 10^{-1}$	$2.65\times 10^{-2}$	$5.08\times 10^{-5}$	$1.47\times 10^{-4}$	$1.35\times 10^{-5}$	$1.46\times 10^{-4}$
	FCC-eh	preselection	$1.89\times 10^{-2}$	$2.00\times 10^{-3}$	$4.25\times 10^{-2}$	$7.30\times 10^{-3}$	$1.64\times 10^{-1}$	$4.16\times 10^{-4}$
		BDT>0.182	$4.14\times 10^{-1}$	$3.86\times 10^{-2}$	$1.99\times 10^{-4}$	$9.77\times 10^{-4}$	$3.65\times 10^{-5}$	$1.93\times 10^{-4}$
60 GeV	LHeC	preselection	$7.72\times 10^{-2}$	$2.17\times 10^{-3}$	$3.22\times 10^{-2}$	$6.78\times 10^{-3}$	$1.48\times 10^{-1}$	$2.14\times 10^{-4}$
		BDT>0.196	$3.05\times 10^{-1}$	$2.93\times 10^{-2}$	$8.25\times 10^{-5}$	$1.26\times 10^{-4}$	$2.70\times 10^{-5}$	$1.46\times 10^{-4}$
	FCC-eh	preselection	$8.20\times 10^{-2}$	$2.00\times 10^{-3}$	$4.25\times 10^{-2}$	$7.30\times 10^{-3}$	$1.64\times 10^{-1}$	$4.16\times 10^{-4}$
		BDT>0.196	$3.94\times 10^{-1}$	$4.59\times 10^{-2}$	$8.76\times 10^{-5}$	$4.14\times 10^{-4}$	$3.65\times 10^{-5}$	$9.64\times 10^{-5}$
120 GeV	LHeC	preselection	$1.48\times 10^{-1}$	$1.56\times 10^{-3}$	$2.76\times 10^{-2}$	$5.66\times 10^{-3}$	$1.33\times 10^{-1}$	$1.49\times 10^{-4}$
		BDT>0.164	$3.79\times 10^{-1}$	$4.14\times 10^{-2}$	$2.15\times 10^{-4}$	$8.41\times 10^{-4}$	$5.40\times 10^{-4}$	$1.26\times 10^{-3}$
	FCC-eh	preselection	$1.49\times 10^{-1}$	$1.46\times 10^{-3}$	$3.80\times 10^{-2}$	$6.40\times 10^{-3}$	$1.55\times 10^{-1}$	$3.19\times 10^{-4}$
		BDT>0.206	$2.52\times 10^{-1}$	$1.30\times 10^{-2}$	$5.35\times 10^{-5}$	$3.42\times 10^{-4}$	$6.44\times 10^{-5}$	$2.51\times 10^{-4}$
200 GeV	LHeC	preselection	$1.94\times 10^{-1}$	$1.56\times 10^{-3}$	$2.76\times 10^{-2}$	$5.66\times 10^{-3}$	$1.33\times 10^{-1}$	$1.49\times 10^{-4}$
		BDT>0.170	$3.23\times 10^{-1}$	$1.92\times 10^{-2}$	$5.70\times 10^{-4}$	$1.90\times 10^{-3}$	$9.16\times 10^{-4}$	$2.10\times 10^{-4}$
	FCC-eh	preselection	$1.96\times 10^{-1}$	$1.46\times 10^{-3}$	$3.80\times 10^{-2}$	$6.40\times 10^{-3}$	$1.55\times 10^{-1}$	$3.19\times 10^{-4}$
		BDT>0.188	$3.19\times 10^{-1}$	$3.20\times 10^{-2}$	$8.29\times 10^{-4}$	$2.46\times 10^{-3}$	$2.58\times 10^{-4}$	$1.25\times 10^{-4}$
600 GeV	LHeC	preselection	$1.98\times 10^{-1}$	$1.56\times 10^{-3}$	$2.76\times 10^{-2}$	$5.66\times 10^{-3}$	$1.33\times 10^{-1}$	$1.49\times 10^{-4}$
		BDT>0.196	$6.42\times 10^{-1}$	$3.60\times 10^{-3}$	$4.81\times 10^{-4}$	$2.29\times 10^{-3}$	$9.76\times 10^{-4}$	$2.10\times 10^{-4}$
	FCC-eh	preselection	$2.01\times 10^{-1}$	$1.46\times 10^{-3}$	$3.80\times 10^{-2}$	$6.40\times 10^{-3}$	$1.55\times 10^{-1}$	$3.19\times 10^{-4}$
		BDT>0.196	$5.52\times 10^{-1}$	$2.96\times 10^{-3}$	$2.49\times 10^{-4}$	$2.73\times 10^{-3}$	$5.80\times 10^{-4}$	$1.25\times 10^{-4}$
1000 GeV	LHeC	preselection	$9.40\times 10^{-2}$	$1.56\times 10^{-3}$	$2.76\times 10^{-2}$	$5.66\times 10^{-3}$	$1.33\times 10^{-1}$	$1.49\times 10^{-4}$
		BDT>0.237	$7.34\times 10^{-1}$	...	$1.11\times 10^{-4}$	$2.19\times 10^{-4}$	$1.35\times 10^{-4}$	$2.10\times 10^{-4}$
	FCC-eh	preselection	$1.35\times 10^{-1}$	$1.46\times 10^{-3}$	$3.80\times 10^{-2}$	$6.40\times 10^{-3}$	$1.55\times 10^{-1}$	$3.19\times 10^{-4}$
		BDT>0.202	$6.17\times 10^{-1}$	$2.37\times 10^{-3}$	$2.05\times 10^{-4}$	$2.55\times 10^{-3}$	$7.08\times 10^{-4}$	$1.25\times 10^{-4}$

**Table 5:** Selection efficiencies of preselection and BDT requirements for both the signal with representative  $m_N$  assumptions and fixing  $|V_{\tau N}|^2 |V_{eN}|^2 / (|V_{\tau N}|^2 + |V_{eN}|^2) = 5 \times 10^{-5}$ , and for background processes at the LHeC and FCC-eh for the hadronic  $\tau_h$  final state, where “...” means the number of events can be reduced to be negligible.

### D.2 Leptonic $\tau_\mu$ final state

$m_N$	collider	selection	signal	$\tau^+\tau^-e^-jjj$	$\tau^+\tau^-\nu_ejjj$	$\tau^+\nu_\tau e^-jjj$	$\tau^+\nu_\tau\nu_ejjj$	$\tau^+\mu^-e^-jjj$	$\mu^+\mu^-\nu_ejjj$	$\mu^+\nu_\mu e^-jjj$	$\mu^+\nu_\mu\nu_ejjj$
20 GeV	LHeC	preselection	$5.27\times 10^{-3}$	$8.70\times 10^{-4}$	$1.77\times 10^{-2}$	$3.65\times 10^{-3}$	$7.30\times 10^{-2}$	$1.83\times 10^{-3}$	$1.67\times 10^{-2}$	$2.80\times 10^{-2}$	$5.93\times 10^{-1}$
		BDT>0.161	$2.84\times 10^{-1}$	$2.85\times 10^{-2}$	$1.61\times 10^{-4}$	$4.43\times 10^{-4}$	...	$1.42\times 10^{-2}$	$1.75\times 10^{-6}$	$2.22\times 10^{-5}$	$3.37\times 10^{-5}$
	FCC-eh	preselection	$9.46\times 10^{-3}$	$8.12\times 10^{-4}$	$2.44\times 10^{-2}$	$3.94\times 10^{-3}$	$4.60\times 10^{-2}$	$8.59\times 10^{-4}$	$2.22\times 10^{-2}$	$2.87\times 10^{-2}$	$3.74\times 10^{-1}$
		BDT>0.151	$4.58\times 10^{-1}$	$5.86\times 10^{-2}$	$4.74\times 10^{-6}$	$7.26\times 10^{-4}$	$1.30\times 10^{-4}$	$6.63\times 10^{-2}$	$3.37\times 10^{-4}$	$1.17\times 10^{-4}$	$8.02\times 10^{-5}$
60 GeV	LHeC	preselection	$3.72\times 10^{-2}$	$8.70\times 10^{-4}$	$1.77\times 10^{-2}$	$3.65\times 10^{-3}$	$7.30\times 10^{-2}$	$1.83\times 10^{-3}$	$1.67\times 10^{-2}$	$2.80\times 10^{-2}$	$5.93\times 10^{-1}$
		BDT>0.139	$3.07\times 10^{-1}$	$2.42\times 10^{-2}$	$1.73\times 10^{-4}$	$6.13\times 10^{-4}$	$2.74\times 10^{-4}$	$9.29\times 10^{-3}$	$2.45\times 10^{-4}$	$4.43\times 10^{-5}$	$5.06\times 10^{-5}$
	FCC-eh	preselection	$4.37\times 10^{-2}$	$8.12\times 10^{-4}$	$2.44\times 10^{-2}$	$3.94\times 10^{-3}$	$4.60\times 10^{-2}$	$8.59\times 10^{-4}$	$2.22\times 10^{-2}$	$2.87\times 10^{-2}$	$3.74\times 10^{-1}$
		BDT>0.153	$4.19\times 10^{-1}$	$4.80\times 10^{-2}$	$2.78\times 10^{-4}$	$7.79\times 10^{-4}$	$5.22\times 10^{-4}$	$4.79\times 10^{-2}$	$4.18\times 10^{-4}$	$9.11\times 10^{-5}$	$9.35\times 10^{-5}$
120 GeV	LHeC	preselection	$7.97\times 10^{-2}$	$6.56\times 10^{-4}$	$1.53\times 10^{-2}$	$3.07\times 10^{-3}$	$6.64\times 10^{-2}$	$1.37\times 10^{-3}$	$1.46\times 10^{-2}$	$2.35\times 10^{-2}$	$5.38\times 10^{-1}$
		BDT>0.120	$3.92\times 10^{-1}$	$3.85\times 10^{-2}$	$6.54\times 10^{-4}$	$2.14\times 10^{-3}$	$2.05\times 10^{-3}$	$5.17\times 10^{-3}$	$5.99\times 10^{-4}$	$1.05\times 10^{-4}$	$8.00\times 10^{-4}$
	FCC-eh	preselection	$8.68\times 10^{-2}$	$5.94\times 10^{-4}$	$2.19\times 10^{-2}$	$3.47\times 10^{-3}$	$4.39\times 10^{-2}$	$6.57\times 10^{-4}$	$1.99\times 10^{-2}$	$2.53\times 10^{-2}$	$3.56\times 10^{-1}$
		BDT>0.139	$5.40\times 10^{-1}$	$9.48\times 10^{-2}$	$1.25\times 10^{-3}$	$3.90\times 10^{-3}$	$2.37\times 10^{-3}$	$7.32\times 10^{-2}$	$1.25\times 10^{-3}$	$3.84\times 10^{-4}$	$5.90\times 10^{-4}$
200 GeV	LHeC	preselection	$1.18\times 10^{-1}$	$6.56\times 10^{-4}$	$1.53\times 10^{-2}$	$3.07\times 10^{-3}$	$6.64\times 10^{-2}$	$1.37\times 10^{-3}$	$1.46\times 10^{-2}$	$2.35\times 10^{-2}$	$5.38\times 10^{-1}$
		BDT>0.118	$3.48\times 10^{-1}$	$3.28\times 10^{-2}$	$2.22\times 10^{-3}$	$5.22\times 10^{-3}$	$6.09\times 10^{-3}$	$5.51\times 10^{-3}$	$2.32\times 10^{-3}$	$7.65\times 10^{-4}$	$2.44\times 10^{-3}$
	FCC-eh	preselection	$1.22\times 10^{-1}$	$5.94\times 10^{-4}$	$2.19\times 10^{-2}$	$3.47\times 10^{-3}$	$4.39\times 10^{-2}$	$6.57\times 10^{-4}$	$1.99\times 10^{-2}$	$2.53\times 10^{-2}$	$3.56\times 10^{-1}$
		BDT>0.125	$4.65\times 10^{-1}$	$1.06\times 10^{-1}$	$4.81\times 10^{-3}$	$1.14\times 10^{-2}$	$7.34\times 10^{-3}$	$5.81\times 10^{-2}$	$5.15\times 10^{-3}$	$2.23\times 10^{-3}$	$3.03\times 10^{-3}$
600 GeV	LHeC	preselection	$1.32\times 10^{-1}$	$6.56\times 10^{-4}$	$1.53\times 10^{-2}$	$3.07\times 10^{-3}$	$6.64\times 10^{-2}$	$1.37\times 10^{-3}$	$1.46\times 10^{-2}$	$2.35\times 10^{-2}$	$5.38\times 10^{-1}$
		BDT>0.252	$1.57\times 10^{-1}$	...	...	...	$3.01\times 10^{-5}$	...	$4.00\times 10^{-5}$	...	$5.58\times 10^{-5}$
	FCC-eh	preselection	$1.32\times 10^{-1}$	$5.94\times 10^{-4}$	$2.19\times 10^{-2}$	$3.47\times 10^{-3}$	$4.39\times 10^{-2}$	$6.57\times 10^{-4}$	$1.99\times 10^{-2}$	$2.53\times 10^{-2}$	$3.56\times 10^{-1}$
		BDT>0.225	$2.05\times 10^{-1}$	...	$4.64\times 10^{-5}$	$2.10\times 10^{-4}$	$2.28\times 10^{-4}$	...	$6.80\times 10^{-5}$	$1.18\times 10^{-4}$	$1.55\times 10^{-4}$
1000 GeV	LHeC	preselection	$6.23\times 10^{-2}$	$6.56\times 10^{-4}$	$1.53\times 10^{-2}$	$3.07\times 10^{-3}$	$6.64\times 10^{-2}$	$1.37\times 10^{-3}$	$1.46\times 10^{-2}$	$2.35\times 10^{-2}$	$5.38\times 10^{-1}$
		BDT>0.266	$3.04\times 10^{-1}$	...	$2.67\times 10^{-5}$	...	...	...	$1.20\times 10^{-4}$	...	$1.86\times 10^{-5}$
	FCC-eh	preselection	$8.80\times 10^{-2}$	$5.94\times 10^{-4}$	$2.19\times 10^{-2}$	$3.47\times 10^{-3}$	$4.39\times 10^{-2}$	$6.57\times 10^{-4}$	$1.99\times 10^{-2}$	$2.53\times 10^{-2}$	$3.56\times 10^{-1}$
		BDT>0.226	$2.34\times 10^{-1}$	...	$3.10\times 10^{-5}$	$1.20\times 10^{-4}$	$9.12\times 10^{-5}$	...	$9.07\times 10^{-5}$	$2.51\times 10^{-4}$	$9.83\times 10^{-5}$

**Table 6:** Similar as Table 5, but for the leptonic  $\tau_\mu$  final state.

## Acknowledgments

We thank Lingxiao Bai for analysing the background of misidentified taus and helpful comments. We also thank Filmon Andom Ghebretinsae, Minglun Tian and Zeren Simon Wang for helpful discussions. H.G. and K.W. are supported by the National Natural Science Foundation of China under grant no. 11905162, the Excellent Young Talents Program of the Wuhan University of Technology under grant no. 40122102, and the research program of the Wuhan University of Technology under grant no. 2020IB024. H.S. is supported by the National Natural Science Foundation of China under grants no. 12075043 and 12147205. Y.N.M. is supported by the National Natural Science Foundation of China under grant no. 12205227 and the Fundamental Research Funds for the Central Universities (WUT: 2022IVA052). The simulation and analysis work of this paper was completed with the computational cluster provided by the Theoretical Physics Group at the Department of Physics, School of Sciences, Wuhan University of Technology.

## References

- [1] Super-Kamiokande, Y. Fukuda *et al.*, Evidence for oscillation of atmospheric neutrinos, Phys. Rev. Lett. **81**, 1562 (1998), arXiv:hep-ex/9807003, BU-98-17, ICRR-REPORT-422-98-18, UCI-98-8, KEK-PREPRINT-98-95, LSU-HEPA-5-98, UMD-98-003, SBHEP-98-5, TKU-PAP-98-06, TIT-HPE-98-09.
- [2] MINOS, D. G. Michael *et al.*, Observation of muon neutrino disappearance with the



- MINOS detectors and the NuMI neutrino beam, Phys. Rev. Lett. **97**, 191801 (2006), arXiv:hep-ex/0607088, FERMILAB-PUB-06-243, BNL-76806-2006-JA.
- [3] MINOS, P. Adamson *et al.*, Improved search for muon-neutrino to electron-neutrino oscillations in MINOS, Phys. Rev. Lett. **107**, 181802 (2011), arXiv:1108.0015, FERMILAB-PUB-11-351-PPD, BNL-96120-2011-JA.
- [4] Double Chooz Collaboration, Y. Abe *et al.*, Indication of reactor  $\bar{\nu}_e$  disappearance in the double chooz experiment, Phys. Rev. Lett. **108**, 131801 (2012), <https://link.aps.org/doi/10.1103/PhysRevLett.108.131801>.
- [5] Daya Bay, J. Ling, Observation of electron-antineutrino disappearance at Daya Bay, AIP Conf. Proc. **1560**, 206 (2013).
- [6] S.-B. Kim, Observation of reactor electron antineutrino disappearance at RENO, Nucl. Phys. B Proc. Suppl. **235-236**, 24 (2013).
- [7] H. Fritzsch, M. Gell-Mann, and P. Minkowski, Vectorlike weak currents and new elementary fermions, Physics Letters B **59**, 256 (1975), <https://www.sciencedirect.com/science/article/pii/0370269375900404>.
- [8] P. Minkowski,  $\mu \rightarrow e\gamma$  at a Rate of One Out of  $10^9$  Muon Decays?, Phys. Lett. B **67**, 421 (1977), Print-77-0182 (BERN).
- [9] T. Yanagida, Horizontal gauge symmetry and masses of neutrinos, Proceedings: Workshop on the Unified Theories and the Baryon Number in the Universe, Conf. Proc. **C7902131**, 95 (1979), KEK-79-18-95.
- [10] O. Sawada and A. Sugamoto, editors, *Proceedings: Workshop on the Unified Theories and the Baryon Number in the Universe: Tsukuba, Japan, February 13-14, 1979*, Tsukuba, Japan, 1979, Natl.Lab.High Energy Phys.
- [11] R. N. Mohapatra and G. Senjanovic, Neutrino Mass and Spontaneous Parity Nonconservation, Phys. Rev. Lett. **44**, 912 (1980), MDDP-TR-80-060, MDDP-PP-80-105, CCNY-HEP-79-10.
- [12] S. L. Glashow, The Future of Elementary Particle Physics, NATO Sci. Ser. B **61**, 687 (1980), HUTP-79-A059.
- [13] M. Gell-Mann, P. Ramond, and R. Slansky, Complex Spinors and Unified Theories, Conf. Proc. **C790927**, 315 (1979), PRINT-80-0576.
- [14] W.-Y. Keung and G. Senjanovic, Majorana Neutrinos and the Production of the Right-handed Charged Gauge Boson, Phys. Rev. Lett. **50**, 1427 (1983), BNL-32872.
- [15] R. Foot, H. Lew, X. G. He, and G. C. Joshi, Seesaw Neutrino Masses Induced by a Triplet of Leptons, Z. Phys. C **44**, 441 (1989), UM-P-88/89, OZ-P-88/7.
- [16] R. N. Mohapatra, Mechanism for Understanding Small Neutrino Mass in Superstring Theories, Phys. Rev. Lett. **56**, 561 (1986).
- [17] M. Magg and C. Wetterich, Neutrino mass problem and gauge hierarchy, Physics Letters B **94**, 61 (1980), <https://www.sciencedirect.com/science/article/pii/0370269380908254>.

- [18] Y. Gao and K. Wang, Heavy neutrino searches via same-sign lepton pairs at a Higgs boson factory, *Phys. Rev. D* **105**, 076005 (2022), arXiv:2102.12826.
- [19] Y. Gao, M. Jin, and K. Wang, Probing the Decoupled Seesaw Scalar in Rare Higgs Decay, *JHEP* **02**, 101 (2020), arXiv:1904.12325.
- [20] S. Antusch, E. Cazzato, O. Fischer, A. Hammad, and K. Wang, Lepton Flavor Violating Dilepton Dijet Signatures from Sterile Neutrinos at Proton Colliders, *JHEP* **10**, 067 (2018), arXiv:1805.11400, DESY 17-151, DESY-17-151.
- [21] C. O. Dib, C. S. Kim, and K. Wang, Signatures of Dirac and Majorana sterile neutrinos in trilepton events at the LHC, *Phys. Rev. D* **95**, 115020 (2017), arXiv:1703.01934, DESY-17-035.
- [22] C. O. Dib, C. S. Kim, and K. Wang, Search for Heavy Sterile Neutrinos in Trileptons at the LHC, *Chin. Phys. C* **41**, 103103 (2017), arXiv:1703.01936, DESY-16-202.
- [23] C. O. Dib, C. S. Kim, K. Wang, and J. Zhang, Distinguishing Dirac/Majorana Sterile Neutrinos at the LHC, *Phys. Rev. D* **94**, 013005 (2016), arXiv:1605.01123, DESY-16-077.
- [24] Z. S. Wang and K. Wang, Physics with far detectors at future lepton colliders, *Phys. Rev. D* **101**, 075046 (2020), arXiv:1911.06576, APCTP Pre2019-024.
- [25] A. Atre, T. Han, S. Pascoli, and B. Zhang, The Search for Heavy Majorana Neutrinos, *JHEP* **05**, 030 (2009), arXiv:0901.3589, FERMILAB-PUB-08-086-T, NSF-KITP-08-54, MADPH-06-1466, DCPT-07-198, IPPP-07-99.
- [26] F. F. Deppisch, P. S. Bhupal Dev, and A. Pilaftsis, Neutrinos and Collider Physics, *New J. Phys.* **17**, 075019 (2015), arXiv:1502.06541, MAN-HEP-2014-15.
- [27] A. Das and N. Okada, Improved bounds on the heavy neutrino productions at the LHC, *Phys. Rev. D* **93**, 033003 (2016), arXiv:1510.04790.
- [28] A. Das, P. Konar, and S. Majhi, Production of Heavy neutrino in next-to-leading order QCD at the LHC and beyond, *JHEP* **06**, 019 (2016), arXiv:1604.00608.
- [29] Y. Cai, T. Han, T. Li, and R. Ruiz, Lepton Number Violation: Seesaw Models and Their Collider Tests, *Front.in Phys.* **6**, 40 (2018), arXiv:1711.02180, PITT-PACC-1712, IPPP-17-74, COEPP-MN-17-17.
- [30] A. Das, Y. Gao, and T. Kamon, Heavy neutrino search via semileptonic Higgs decay at the LHC, *Eur. Phys. J. C* **79**, 424 (2019), arXiv:1704.00881, WSU-HEP-1706, MI-TH-1748.
- [31] P. D. Bolton, F. F. Deppisch, and P. S. Bhupal Dev, Neutrinoless double beta decay versus other probes of heavy sterile neutrinos, *JHEP* **03**, 170 (2020), arXiv:1912.03058.
- [32] J.-N. Ding, Q. Qin, and F.-S. Yu, Heavy neutrino searches at future  $Z$ -factories, *Eur. Phys. J. C* **79**, 766 (2019), arXiv:1903.02570, SI-HEP-2019-02, QFET-2019-02.
- [33] Y.-F. Shen, J.-N. Ding, and Q. Qin, Monojet search for heavy neutrinos at future  $Z$ -factories, *Eur. Phys. J. C* **82**, 398 (2022), arXiv:2201.05831.
- [34] L3, M. Acciarri *et al.*, Search for heavy isosinglet neutrinos in  $e^+e^-$  annihilation at 130-GeV less than  $S^{(1/2)}$  less than 189-GeV, *Phys. Lett. B* **461**, 397 (1999), arXiv:hep-ex/9909006, CERN-EP-99-083, CERN-EP-99-83.

- [35] L3, P. Achard *et al.*, Search for heavy isosinglet neutrino in  $e^+e^-$  annihilation at LEP, Phys. Lett. B **517**, 67 (2001), arXiv:hep-ex/0107014, CERN-EP-2001-045.
- [36] CMS, A. M. Sirunyan *et al.*, Search for heavy neutral leptons in events with three charged leptons in proton-proton collisions at  $\sqrt{s} = 13$  TeV, Phys. Rev. Lett. **120**, 221801 (2018), arXiv:1802.02965, CMS-EXO-17-012, CERN-EP-2018-006.
- [37] CMS, A. M. Sirunyan *et al.*, Search for heavy Majorana neutrinos in same-sign dilepton channels in proton-proton collisions at  $\sqrt{s} = 13$  TeV, JHEP **01**, 122 (2019), arXiv:1806.10905, CMS-EXO-17-028, CERN-EP-2018-159.
- [38] CMS, Search for long-lived heavy neutral leptons with displaced vertices in pp collisions at  $\sqrt{s} = 13$  TeV with the CMS detector, (2021), CMS-PAS-EXO-20-009.
- [39] ATLAS, G. Aad *et al.*, Search for heavy neutral leptons in decays of  $W$  bosons produced in 13 TeV  $pp$  collisions using prompt and displaced signatures with the ATLAS detector, JHEP **10**, 265 (2019), arXiv:1905.09787, CERN-EP-2019-071.
- [40] LHCb, R. Aaij *et al.*, Search for heavy neutral leptons in  $W^+ \rightarrow \mu^+ \mu^\pm \text{jet}$  decays, Eur. Phys. J. C **81**, 248 (2021), arXiv:2011.05263, LHCb-PAPER-2020-022, CERN-EP-2020-194.
- [41] NA62, E. Cortina Gil *et al.*, Search for heavy neutral lepton production in  $K^+$  decays to positrons, Phys. Lett. B **807**, 135599 (2020), arXiv:2005.09575, CERN-EP-2020-089.
- [42] Belle, D. Liventsev *et al.*, Search for heavy neutrinos at Belle, Phys. Rev. D **87**, 071102 (2013), arXiv:1301.1105, [Erratum: Phys.Rev.D 95, 099903 (2017)], BELLE-PREPRINT-2012-28, KEK-PREPRINT-2012-32.
- [43] T2K, K. Abe *et al.*, Search for heavy neutrinos with the T2K near detector ND280, Phys. Rev. D **100**, 052006 (2019), arXiv:1902.07598.
- [44] CMS, Probing heavy Majorana neutrinos and the Weinberg operator through vector boson fusion processes in proton-proton collisions at  $\sqrt{s} = 13$  TeV, (2022), arXiv:2206.08956, CMS-EXO-21-003, CERN-EP-2022-105.
- [45] H. Gu and K. Wang, Search for heavy Majorana neutrinos at electron-proton colliders, Phys. Rev. D **106**, 015006 (2022), arXiv:2201.12997.
- [46] DELPHI, P. Abreu *et al.*, Search for neutral heavy leptons produced in Z decays, Z. Phys. C **74**, 57 (1997), [Erratum: Z.Phys.C 75, 580 (1997)], CERN-PPE-96-195.
- [47] F. de lAguila, J. de Blas, and M. Perez-Victoria, Effects of new leptons in Electroweak Precision Data, Phys. Rev. D **78**, 013010 (2008), arXiv:0803.4008, UG-FT-224-08, CAFPE-94-08.
- [48] E. Akhmedov, A. Kartavtsev, M. Lindner, L. Michaels, and J. Smirnov, Improving Electro-Weak Fits with TeV-scale Sterile Neutrinos, JHEP **05**, 081 (2013), arXiv:1302.1872.
- [49] L. Basso, O. Fischer, and J. J. van der Bij, Precision tests of unitarity in leptonic mixing, EPL **105**, 11001 (2014), arXiv:1310.2057, FR-PHENO-2013-012.
- [50] J. de Blas, Electroweak limits on physics beyond the Standard Model, EPJ Web Conf. **60**, 19008 (2013), arXiv:1307.6173.
- [51] S. Antusch and O. Fischer, Testing sterile neutrino extensions of the Standard Model at future lepton colliders, JHEP **05**, 053 (2015), arXiv:1502.05915, MPP-2015-24.

- [52] M. Chrzaszcz *et al.*, A frequentist analysis of three right-handed neutrinos with GAMBIT, *Eur. Phys. J. C* **80**, 569 (2020), arXiv:1908.02302, gambit-physics-2019.
- [53] K. Cheung, Y.-L. Chung, H. Ishida, and C.-T. Lu, Sensitivity reach on heavy neutral leptons and  $\tau$ -neutrino mixing  $|U_{\tau N}|^2$  at the HL-LHC, *Phys. Rev. D* **102**, 075038 (2020), arXiv:2004.11537.
- [54] K. Bondarenko, A. Boyarsky, D. Gorbunov, and O. Ruchayskiy, Phenomenology of GeV-scale Heavy Neutral Leptons, *JHEP* **11**, 032 (2018), arXiv:1805.08567.
- [55] G. Cvetič and C. S. Kim, Sensitivity bounds on heavy neutrino mixing  $|U_{\mu N}|^2$  and  $|U_{\tau N}|^2$  from LHCb upgrade, *Phys. Rev. D* **100**, 015014 (2019), arXiv:1904.12858, USM-TH-361.
- [56] C. O. Dib *et al.*, Searching for a sterile neutrino that mixes predominantly with  $\nu_\tau$  at  $B$  factories, *Phys. Rev. D* **101**, 093003 (2020), arXiv:1908.09719.
- [57] G. Zhou, J. Y. Günther, Z. S. Wang, J. de Vries, and H. K. Dreiner, Long-lived sterile neutrinos at Belle II in effective field theory, *JHEP* **04**, 057 (2022), arXiv:2111.04403, BONN-TH-2021-11.
- [58] A. Abada, N. Bernal, M. Losada, and X. Marcano, Inclusive Displaced Vertex Searches for Heavy Neutral Leptons at the LHC, *JHEP* **01**, 093 (2019), arXiv:1807.10024, LPT-ORSAY-18-79, PI/UAN-2018-631FT.
- [59] G. Cottin, J. C. Helo, and M. Hirsch, Displaced vertices as probes of sterile neutrino mixing at the LHC, *Phys. Rev. D* **98**, 035012 (2018), arXiv:1806.05191, IFIC/18-25, IFIC-18-25.
- [60] A. Flórez, K. Gui, A. Gurrola, C. Patiño, and D. Restrepo, Expanding the Reach of Heavy Neutrino Searches at the LHC, *Phys. Lett. B* **778**, 94 (2018), arXiv:1708.03007.
- [61] S. Pascoli, R. Ruiz, and C. Weiland, Safe Jet Vetoes, *Phys. Lett. B* **786**, 106 (2018), arXiv:1805.09335, IPPP/18/36, IPPP-18-36.
- [62] S. Pascoli, R. Ruiz, and C. Weiland, Heavy neutrinos with dynamic jet vetoes: multilepton searches at  $\sqrt{s} = 14, 27, \text{ and } 100$  TeV, *JHEP* **06**, 049 (2019), arXiv:1812.08750, CP3-18-77, IPPP/18/111, PITT-PACC-1821, VBSCAN-PUB-10-18.
- [63] L. Bai, Y.-n. Mao, and K. Wang, Probe the Mixing Parameter  $|V_{\tau N}|^2$  for Heavy Neutrinos, (2022), arXiv:2211.00309.
- [64] LHeC/FCC-eh Study Group, G. Azuelos, M. D’Onofrio, and O. Fischer, Beyond Standard Model Physics at the LHeC and the FCC-eh, *PoS ICHEP2020*, 227 (2021).
- [65] M. Klein, The Large Hadron Electron Collider Project, in *17th International Workshop on Deep-Inelastic Scattering and Related Subjects*, p. 236, 2009, arXiv:0908.2877.
- [66] LHeC Study Group, J. L. Abelleira Fernandez *et al.*, A Large Hadron Electron Collider at CERN: Report on the Physics and Design Concepts for Machine and Detector, *J. Phys. G* **39**, 075001 (2012), arXiv:1206.2913, SLAC-R-999, CERN-OPEN-2012-015, LHEC-NOTE-2012-001-GEN.
- [67] O. Bruening and M. Klein, The Large Hadron Electron Collider, *Mod. Phys. Lett. A* **28**, 1330011 (2013), arXiv:1305.2090, LHEC-NOTE-2013-001-GEN.
- [68] M. Klein, Deep inelastic scattering at the energy frontier, *Annalen Phys.* **528**, 138 (2016).

- [69] LHeC, FCC-he Study Group, P. Agostini *et al.*, The Large Hadron-Electron Collider at the HL-LHC, *J. Phys. G* **48**, 110501 (2021), arXiv:2007.14491, CERN-ACC-Note-2020-0002, JLAB-ACP-20-3180.
- [70] LHeC, FCC-eh Study Group, B. Holzer and K. D. J. André, Energy Frontier DIS at CERN: the LHeC and the FCC-eh, PoS **ICHEP2020**, 687 (2021).
- [71] F. Zimmermann, M. Benedikt, D. Schulte, and J. Wenninger, Challenges for Highest Energy Circular Colliders, in *5th International Particle Accelerator Conference*, p. MOXAA01, 2014.
- [72] R. Tomás *et al.*, Fcc study: parameters and optics for hadron and lepton colliders, *Nuclear and Particle Physics Proceedings* **273-275**, 149 (2016), 37th International Conference on High Energy Physics (ICHEP), <https://www.sciencedirect.com/science/article/pii/S2405601415005076>.
- [73] FCC, A. Abada *et al.*, FCC Physics Opportunities: Future Circular Collider Conceptual Design Report Volume 1, *Eur. Phys. J. C* **79**, 474 (2019), CERN-ACC-2018-0056.
- [74] S. Antusch, A. Hammad, and A. Rashed, Probing  $Z'$  mediated charged lepton flavor violation with taus at the LHeC, *Phys. Lett. B* **810**, 135796 (2020), arXiv:2003.11091.
- [75] W. Buchmüller and C. Greub, Electroproduction of majorana neutrinos, *Physics Letters B* **256**, 465 (1991), <https://www.sciencedirect.com/science/article/pii/037026939191792T>.
- [76] W. Buchmuller and C. Greub, Heavy Majorana neutrinos in electron - positron and electron - proton collisions, *Nucl. Phys. B* **363**, 345 (1991), DESY-91-034.
- [77] W. Buchmuller and C. Greub, Right-handed currents and heavy neutrinos in high-energy  $ep$  and  $e^+e^-$  scattering, *Nucl. Phys. B* **381**, 109 (1992), DESY-92-023, ZU-TH-9-92.
- [78] G. Ingelman and J. Rathsman, Heavy Majorana neutrinos at e p colliders, *Z. Phys. C* **60**, 243 (1993), DESY-93-039, TSL-ISV-93-0081.
- [79] F. M. L. de Almeida, Y. do Amaral Coutinho, J. A. Martins Simoes, and M. A. B. do Vale, Heavy majorana neutrinos at a very large electron proton collider, *Phys. Rev. D* **65**, 115010 (2002).
- [80] H. Liang, X.-G. He, W.-G. Ma, S.-M. Wang, and R.-Y. Zhang, Seesaw Type I and III at the LHeC, *JHEP* **09**, 023 (2010), arXiv:1006.5534.
- [81] C. Blaksley, M. Blennow, F. Bonnet, P. Coloma, and E. Fernandez-Martinez, Heavy Neutrinos and Lepton Number Violation in lp Colliders, *Nucl. Phys. B* **852**, 353 (2011), arXiv:1105.0308, CERN-PH-TH-2011-094, EURONU-WP6-11-32, IFT-UAM-CSIC-11-25, MPP-2011-50.
- [82] L. Duarte, G. A. González-Sprinberg, and O. A. Sampayo, Majorana neutrinos production at LHeC in an effective approach, *Phys. Rev. D* **91**, 053007 (2015), arXiv:1412.1433.
- [83] S. Mondal and S. K. Rai, Probing the Heavy Neutrinos of Inverse Seesaw Model at the LHeC, *Phys. Rev. D* **94**, 033008 (2016), arXiv:1605.04508, HRI-RECAPP-2016-009.
- [84] S. Antusch, E. Cazzato, and O. Fischer, Sterile neutrino searches at future  $e^-e^+$ ,  $pp$ , and  $e^-p$  colliders, *Int. J. Mod. Phys. A* **32**, 1750078 (2017), arXiv:1612.02728.

- [85] M. Lindner, F. S. Queiroz, W. Rodejohann, and C. E. Yaguna, Left-Right Symmetry and Lepton Number Violation at the Large Hadron Electron Collider, *JHEP* **06**, 140 (2016), arXiv:1604.08596.
- [86] S.-Y. Li, Z.-G. Si, and X.-H. Yang, Heavy Majorana Neutrino Production at Future  $ep$  Colliders, *Phys. Lett. B* **795**, 49 (2019), arXiv:1811.10313.
- [87] A. Das, S. Jana, S. Mandal, and S. Nandi, Probing right handed neutrinos at the LHeC and lepton colliders using fat jet signatures, *Phys. Rev. D* **99**, 055030 (2019), arXiv:1811.04291, OSU-HEP-18-06.
- [88] S. Antusch, O. Fischer, and A. Hammad, Lepton-Trijet and Displaced Vertex Searches for Heavy Neutrinos at Future Electron-Proton Colliders, *JHEP* **03**, 110 (2020), arXiv:1908.02852.
- [89] G. Cottin, O. Fischer, S. Mandal, M. Mitra, and R. Padhan, Displaced Neutrino Jets at the LHeC, (2021), arXiv:2104.13578.
- [90] B. Batell, T. Ghosh, T. Han, and K. Xie, Heavy Neutral Leptons at the Electron-Ion Collider, (2022), arXiv:2210.09287, HRI-RECAPP-2022-006, PITT-PACC-2107.
- [91] D. Alva, T. Han, and R. Ruiz, Heavy Majorana neutrinos from  $W\gamma$  fusion at hadron colliders, *JHEP* **02**, 072 (2015), arXiv:1411.7305, PITT-PACC-1407.
- [92] C. Degrande, O. Mattelaer, R. Ruiz, and J. Turner, Fully-Automated Precision Predictions for Heavy Neutrino Production Mechanisms at Hadron Colliders, *Phys. Rev. D* **94**, 053002 (2016), arXiv:1602.06957, IPPP-16-13, MCNET-16-05.
- [93] J. Alwall *et al.*, The automated computation of tree-level and next-to-leading order differential cross sections, and their matching to parton shower simulations, *JHEP* **07**, 079 (2014), arXiv:1405.0301, CERN-PH-TH-2014-064, CP3-14-18, LPN14-066, MCNET-14-09, ZU-TH-14-14.
- [94] G. Azuelos, M. D’Onofrio, S. Iwamoto, and K. Wang, Search for the SUSY electroweak sector at  $ep$  colliders, *Phys. Rev. D* **101**, 095015 (2020), arXiv:1912.03823.
- [95] T. Sjostrand, S. Mrenna, and P. Z. Skands, PYTHIA 6.4 Physics and Manual, *JHEP* **05**, 026 (2006), arXiv:hep-ph/0603175, FERMILAB-PUB-06-052-CD-T, LU-TP-06-13.
- [96] LHeC and FCC-eh Delphes card files, [https://github.com/delphes/delphes/blob/master/cards/delphes\\_card\\_LHeC.tcl](https://github.com/delphes/delphes/blob/master/cards/delphes_card_LHeC.tcl), [https://github.com/delphes/delphes/blob/master/cards/delphes\\_card\\_FCCeh.tcl](https://github.com/delphes/delphes/blob/master/cards/delphes_card_FCCeh.tcl).
- [97] DELPHES 3, J. de Favereau *et al.*, DELPHES 3, A modular framework for fast simulation of a generic collider experiment, *JHEP* **02**, 057 (2014), arXiv:1307.6346.
- [98] M. Cacciari, G. P. Salam, and G. Soyez, FastJet User Manual, *Eur. Phys. J. C* **72**, 1896 (2012), arXiv:1111.6097, CERN-PH-TH-2011-297.
- [99] A. Hocker *et al.*, TMVA - Toolkit for Multivariate Data Analysis, (2007), arXiv:physics/0703039, CERN-OPEN-2007-007.
- [100] G. Cowan, Discovery sensitivity for a counting experiment with background uncertainty, (2012), <http://www.pp.rhul.ac.uk/~cowan/stat/medsig/medsigNote.pdf>.

- [101] ATLAS, Formulae for Estimating Significance, (2020), ATL-PHYS-PUB-2020-025.
- [102] P. N. Bhattiprolu, S. P. Martin, and J. D. Wells, Criteria for projected discovery and exclusion sensitivities of counting experiments, *Eur. Phys. J. C* **81**, 123 (2021), arXiv:2009.07249.
- [103] Particle Data Group, P. Zyla *et al.*, Review of Particle Physics, *PTEP* **2020**, 083C01 (2020).
- [104] Particle Data Group, R. L. Workman *et al.*, Review of Particle Physics, *PTEP* **2022**, 083C01 (2022).
- [105] CDF, D0, T. A. Aaltonen *et al.*, Tevatron Run II combination of the effective leptonic electroweak mixing angle, *Phys. Rev. D* **97**, 112007 (2018), arXiv:1801.06283, FERMILAB-PUB-18-015-E.
- [106] ATLAS, Measurement of the effective leptonic weak mixing angle using electron and muon pairs from  $Z$ -boson decay in the ATLAS experiment at  $\sqrt{s} = 8$  TeV, (2018), ATLAS-CONF-2018-037.